DIRECT MEASUREMENT OF SKIN FRICTION ON MAGNETICALLY LEVITATED VEHICLES

By

Alexei Vladimirovich Marshakov

A Thesis Submitted to the Faculty of

Virginia Polytechnic Institute and State University

in Partial Fulfillment of the Requirements for the Degree

of Master of Science

in

Aerospace Engineering

Joseph A. Schetz,
Chairman

James F. Marchman, III

Roger L. Simpson

April 1996

Blacksburg, Virginia

Keywords: aerodynamics, friction, sensor

DIRECT MEASUREMENT OF SKIN FRICTION ON MAGNETICALLY LEVITATED VEHICLES

By

Alexei Vladimirovich Marshakov

Joseph A. Schetz, Chairman

Department of Aerospace and Ocean Engineering

(ABSTRACT)

The goal to design and build a reliable instrument for the direct measurement of skin friction on the surface of Magnetically Levitated (MagLev) trains was successfully achieved. A wall mounted, cantilevered beam device was used to measure the small tangential flow shear force that passes over the non-intrusive floating element. Piezoresistive strain gage units measure the relatively small strain that is generated by the wall shear. By adapting the geometry of the sensing unit, this design can be adapted for a variety of test flows. Measurements were made on two different vehicle geometries provided by Northrop/Grumman and Lockheed/Martin as well as on a special

model designed to study the influence of propulsion rails on the Lockheed/Martin model aerodynamics. The obtained values of the skin friction coefficient C_f are deemed reasonable for the type of flow studied. The estimated uncertainty of the gage is ± 5.2%. The data agreed to within 10% with estimated values from an idealized Couette flow analysis.

ACKNOWLEDGMENTS

First, I want to express my sincerest gratitude to Dr. Joseph A. Schetz for giving me this wonderful research and study opportunity, for his patience and genuine concern.

Second, I would like to thank Dr. and Mrs. Chester W. Spencer for becoming my American family and for their generous support and care for the past several years.

Special thanks to the members of AOE machine shop, including Bruce Stanger, Greg Dudding and Kent Morris and to Gary Stafford for their help and advise.

I must also thank my fellow graduate students for their help, support and friendship.

Finally, my sincerest thanks to my wife Olga for her support and encouragement.

NOMENCLATURE

A	Area
C_f	Skin Friction Coefficient
h	height
M	Mach Number
q	Dynamic Pressure
R	Resistance
Re	Reynolds Number (based on length of the model)
t	time
U	velocity
V	Voltage
u^*	Friction Velocity
X	Axial distance
y	Normal ditance to the wall
κ	Clauser Constant
μ	Viscosity
ν	Kinematic Viscosity
ρ	Density
τ	Shear Stress

Subscripts

w	Condition at the Wall
T	Turbulent

CONTENTS

LIST OF FIGURES

LIST OF TABLES

1. INTRODUCTION

BACKGROUND

A knowledge of the drag resulting from skin friction is important for several reasons, both scientific and practical. Scientifically, the skin friction is a key component in determining the friction velocity,

$$u^* = \sqrt{\frac{\tau_w}{\rho_w}}$$

that is used as the scaling velocity in the correlation of turbulent boundary layer profiles. From a more practical perspective, skin friction is important to the performance of virtually all fluid machinery systems and components. Skin friction plays a key role in drag of any vehicle moving at relatively high speed.

The measurement of skin friction is not a new science. Skin friction has been successfully measured for years using indirect and direct methods. Most laminar flow situations have reliable skin friction measurements available and a host of prediction methods are available for simple flows over a flat plate. The measurement of skin friction can be classified into two categories of techniques-- indirect or direct methods.

Indirect methods involve measurement of the boundary layer velocity gradient or heat transfer along with some assumptions so that the skin friction can be inferred. Nitsche et al [1] present a thorough review of many of these methods and their strategies. Wooden [2] presents in

tabular form a list of advantages and disadvantages of several types of experimental skin friction measurements. Wooden and Hull treat Reynolds Analogy measurements as a separate method as he considers the physical quantity being measured (i.e., force, total pressure, and heat transfer) as his dividing criterion. In this discussion, however, Reynolds Analogy will be considered a subset of indirect methods.

Figure 1 that comes from the work of Nitsche et al.[1] summarizes most of the indirect techniques used for the skin friction measurements along with their underlying principles.

First technique involves the use of heated wires or films along the wall in order to measure heat transfer. In 1874, Osborne Reynolds suggested that the mechanism between the heat transfer and momentum transfer in a turbulent boundary layer are similar. This conclusion leads to the Reynolds Analogy - a relationship between the skin friction coefficient and the heat transfer coefficient. The Reynolds Analogy can be expressed as [3]:

$$St\,\mathrm{Pr}^{\frac{2}{3}} = \frac{C_f}{2}$$

or simply as

$$St = \frac{C_f}{2}$$

in the case of turbulent Prandtl number of unity. Reynolds' theory has been modified by various researchers as given in Wooden [2] which follows from Rubesin [4]. These empirical modifications and corrections refine the calibrations for this type of flows. Only the basic Reynolds Analogy technique for a surface hot film sensor will be discussed here

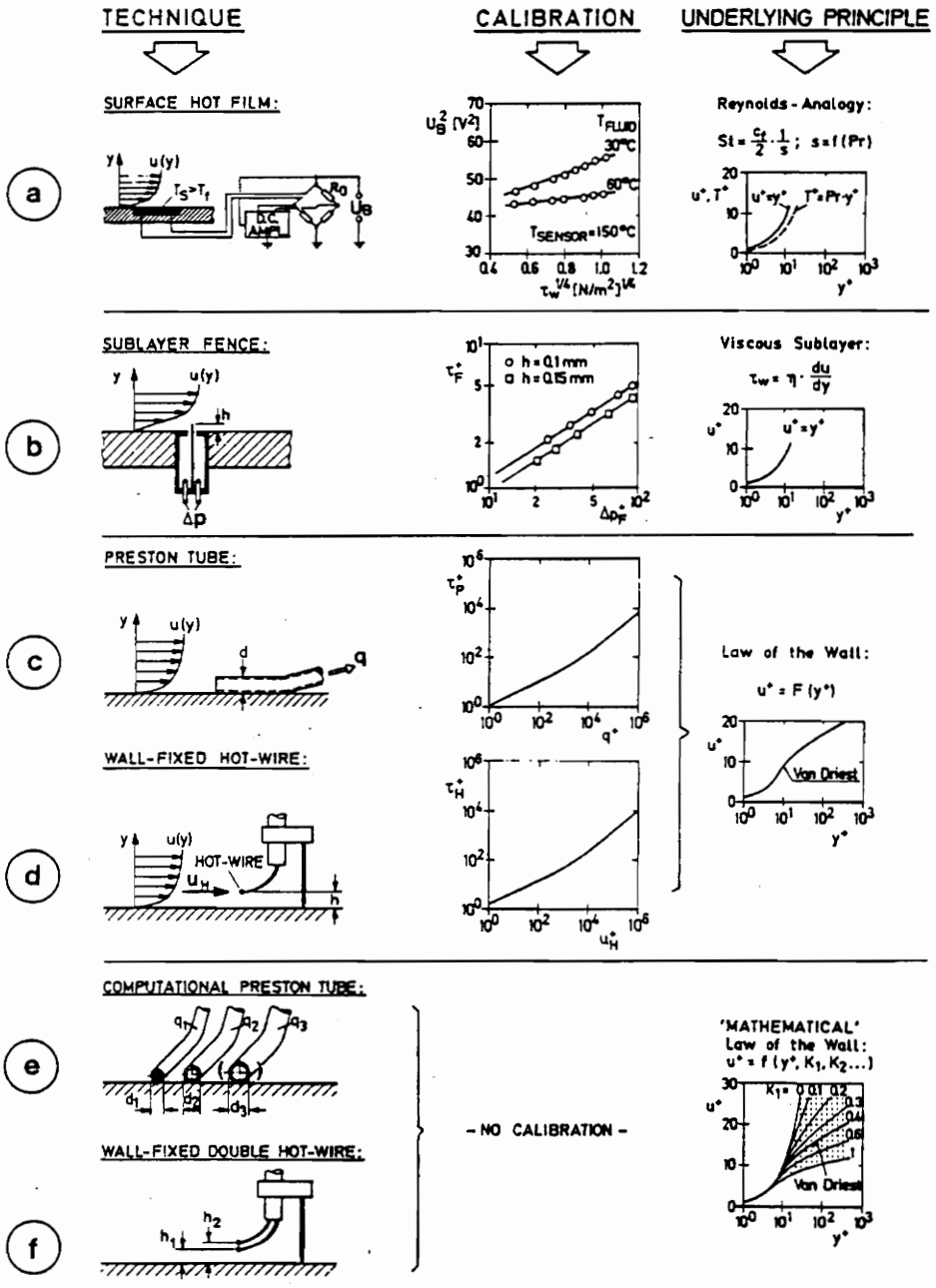

Figure 1. Indirect shear stress measurement techniques

The surface hot film sensor technique (Fig. 1a) is based on the concept that convective losses of a small heated sensor mounted on the wall and maintained at constant temperature can be correlated to the wall shear stress. The empirical calibration formula is usually in the form:

$$U_B^2 = A + B\tau_w^n$$

were U_B is the bridge voltage. Several researchers have measured skin friction with such a technique[5], [6], [7]. The technique does well in cases where Reynolds Analogy may be applied. Bellhouse and Schultz [8] raised concerns for use of a heated film.

Another indirect technique is the sublayer fence (Fig. 1b). This method is based on the similarity law of the viscous sublayer. The measured differential pressure at the fence is correlated to the local shear force using the relationship between this pressure and the velocity close to the wall.

Among the most widely used indirect methods is the Preston tube, as shown in Figure 1c.

The Preston tube operates by resting a small tube on the wall surface in order to measure the Pitot pressure. The tube's size allows the probe to sense the viscous sublayer, the buffer layer and the logarithmic portion of the boundary layer, meaning that the complete law of the wall must be supposed when utilizing this technique. The relation between the wall shear and measured dynamic pressure in the probe is usually represented by an empirical calibration curve which is a fit through a logarithmic law. The problem with such an arrangement is that direct relationship between the law of the wall and the calibration method indicate that measurement of skin friction by a Preston tube technique will break down in situations that

lead to a deviation from the law of the wall. Thus the Preston tube will fail in such flows as a transition region or separating and reattaching flows as the law of the wall breaks down. Furthermore, it will be of very limited use in a three-dimensional flow regime as well.

Similar in principle to the Preston tube, a Stanton tube[9] consists of a Pitot tube with a rectangular opening. A Stanton tube can easily be fabricated by placing a piece of razor blade over a static pressure hole. A schematic drawing of a Stanton tube is shown in Figure 2.

While being very similar, there are some important differences between Stanton and Preston tubes. First, the Preston tube is a global device which measures Bernoulli-type pressures. These pressures are a result of the deceleration of fluid in front of the tube. The Stanton tube, being a local device, does not respond to Bernoulli-type pressures. This enables it to respond more quickly to local shear stress fluctuations. Second, Stanton tubes are characterized by numerous physical parameters such as width and overall height of the device and the flow entrance opening. That makes the calculation of the wall shear levels much more tedious than those of the Preston tube.

However, the Stanton tube must be compensated as well when utilized in three-dimensional flows or flows with pressure gradient since the velocity profile will be changed. Likewise, a hot-wire at a fixed distance above the wall can be utilized in the logarithmic region to determine the velocity u at a distance h above the wall. However, although this method is less sensitive to changed wall laws, it still has the same restrictions as the Preston tube method.

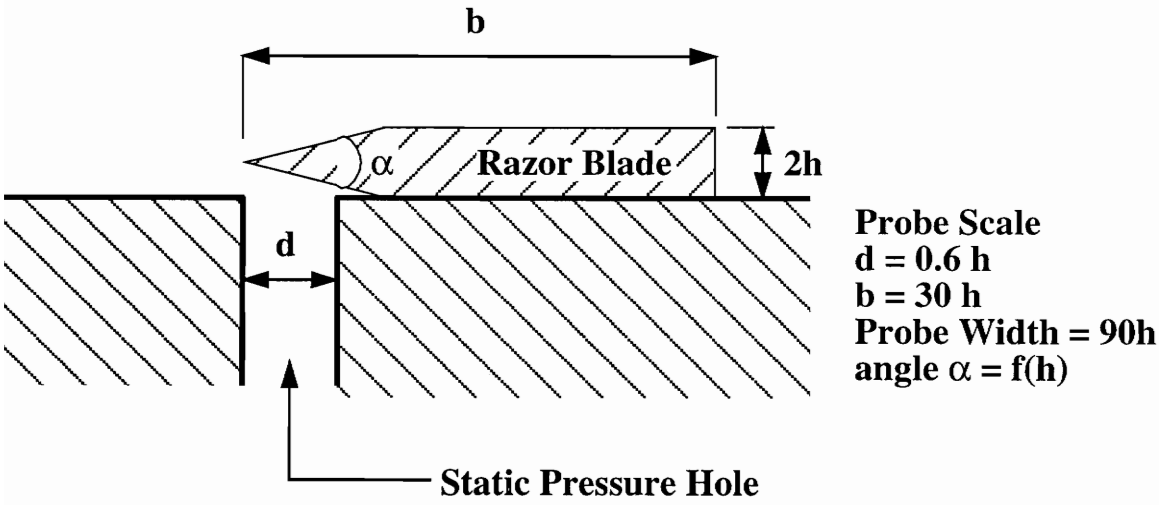

Figure 2. Stanton Tube Technique

The other techniques shown in Figure 1 including wall-fixed hot wire, computational Preston tube and wall-fixed double hot wire are, basically, modified basic methods described above adopted for measurements in certain flow conditions.

A final indirect technique involves the use of liquid crystals to qualitatively and quantitatively measure skin friction[10]. Liquid crystals are optically active mixtures which have the ability to reflect light of a particular wavelength which changes in response to a certain physical stimuli.

By making the crystals sensitive to shear stress, a calibration curve can be generated which relates the shear stress to reflected wavelength. However, liquid crystals are still much more suited to indicating transition location than reporting skin friction measurements.

Before going into a discussion of the direct methods, a brief survey of what will be called semi-direct or quasi-direct methods will be made. Among these would be the use of a thin liquid film[11] which is placed on the surface of the body and deformed by the gas flow over it. Hence, the term semi-direct method as the film is placed on the body rather than in the body as a floating-element gage would be.

The concept behind a thin film technique is that the surface shear stress can be deduced from the rate of deformation of the thin oil film based upon lubrication theory. The shear stress can be assumed to be the primary force on the film if the film is thin relative to its length, there is little surface curvature, and the flow is unaffected by the film's presence. If one has the ability to measure the deformation of the thin oil film over time, then it is possible to accurately determine the skin friction based upon a characteristic film profile.

For the case of Seto's [12] experiment, the characteristic film profile for constant shear stress, zero pressure gradient two-dimensional flow was:

$$y = \frac{\mu x}{\tau t}$$

where y is the film thickness, μ is the viscosity, x is the distance from the leading edge of the film, τ is the shear stress and t is the time. A schematic drawing of such a profile can be seen in Figure 3. The linear profile above occurs in the limiting case of increasing time and decreasing film thickness. So for a very thin film case, the influence of the film on the flow is negligible and the above equation gives a direct relation between the shear stress and the film thickness and deformation.

Several researchers have different methods for measuring the deformation of the oil. Tanner [13] used laser interferometric thickness measurements of the oil thickness. A non-intrusive double laser beam interferometer system was developed as an advancement to Tanner's arrangement [14]. These methods were further improved by O'Brien [15] who placed microspheres on the surface of the film and imaged their motion through a microscope beneath the flow. Other researchers utilize other techniques for visualizing the oil deformation[12].These techniques are very successful at measuring skin friction on a flat plate in a non-intrusive manner. However, it is likely that the model may be in motion on the test stand and the optical access might be limited.

Direct force measurement techniques generally include two types of force balances - nulling and non-nulling. In the nulling design, the sensing element, a small movable portion of the wall, is acted upon by the shearing force but it is not deflected (see Figure 4). Instead, it is held

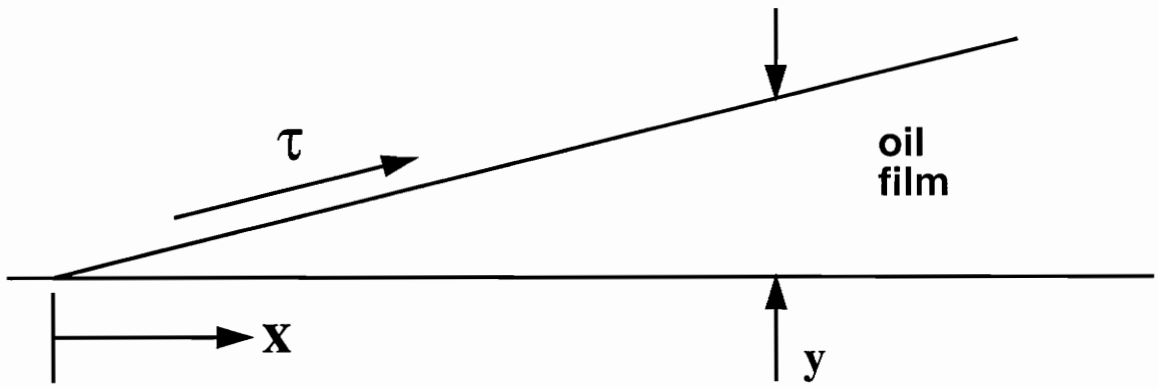

Figure 3. Oil Film Profile

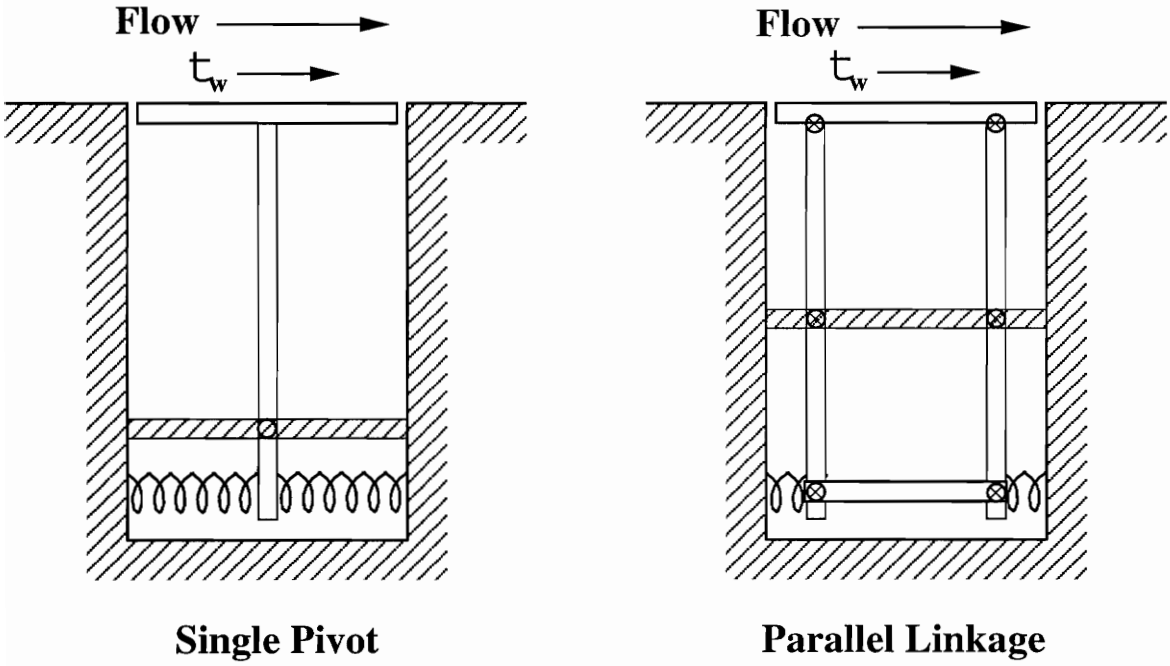

Figure 4. The Scheme of the Nulling Gage

fixed in its initial position by a restoring force that is equal to the shear force. In the non-nulling design, the sensing element is allowed to deflect under the shearing load. This type of design is much simpler than a self-nulling design, however it introduces some concern as the deflection allows the sensing head to tilt and protrude into the flow and it permits the sensor geometry to vary.

Winter [16] presents a history of early direct measurement designs.

Many of the nulling gages are mechanically complex, using some parallel linkage arrangement to sense the force on the floating element. That is, the sensing element does not move but instead transfers the force through the parallel linkage which measures the amount of compensating force required to keep the element stationary. A schematic drawing of such a design from Allen [17] can be seen in Figure 4. Vakili [18] has come up with a moving belt technique called a Belt Skin Friction Balance (BSFB). As shown in Figure 5, this gage functions by having a flexible belt wrapped tightly around two cylinders with parallel axes. As the flow goes over the belt, the shear force applied to the belt forces the cylinders to rotate a very small amount. Strain gages installed on the flexure measure the strain which is proportional to the belt's deflection.

A nulling device is attractive for many reasons, since it is a direct measurement with no assumptions regarding the properties of the flow and the balance remains fixed and will not alter the flow. Many nulling designs exist for measuring skin friction. However, there are some drawbacks to the nulling design. The mechanical complexity can present a problem with fabrication and susceptibility to error. Last, a nulling design has a much slower time response compared to non-nulling scheme.

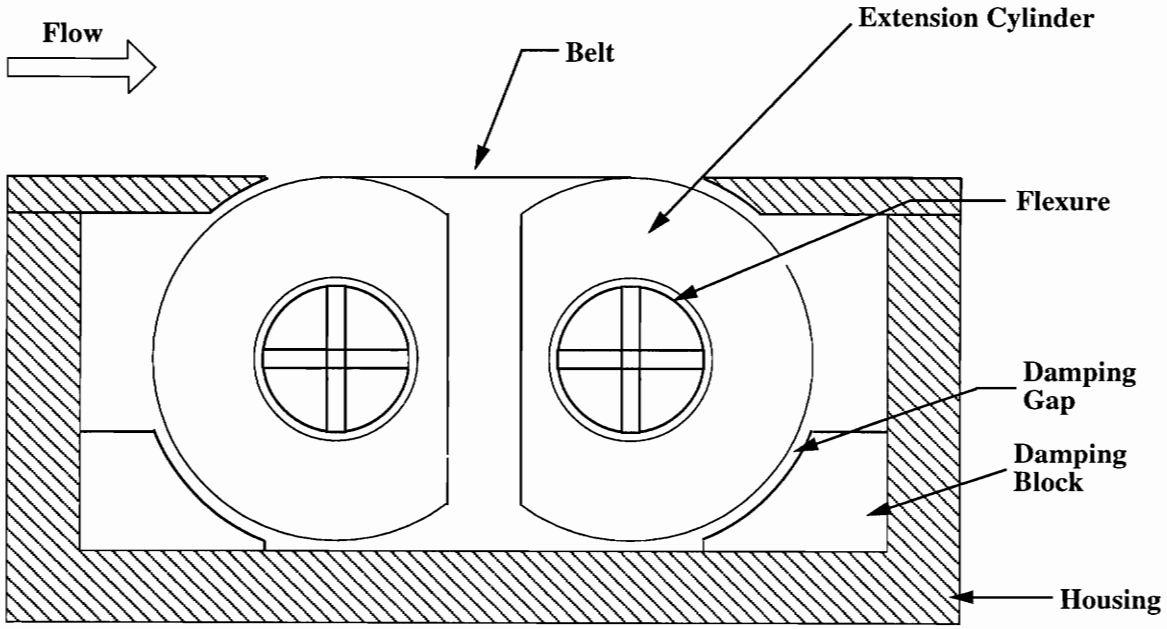

Figure 5. The Scheme of Belt Skin Friction Gage

Thus, we come to the non-nulling direct measurement method for a skin friction balance in the hopes that this configuration will be successful for the applications of interest here. The non-nulling device allows the cantilevered floating element to move a very small distance, and the bending at the base of the beam can be measured. This is mechanically much simpler than the nulling design, and consequently less susceptible to errors.

This kind of design was first use in the cantilever arrangement by Schetz and Nerney [19]. Their design was made possible by use of very sensitive crystal strain gages. The concept of a non-nulling instrument using crystal strain gages allows measurement of the small surface shear forces with very small deflections of the sensing head. For these very small deflections the tilting of the head is small enough so that the errors due to misalignment are minimal. References [20] and [21] also present data obtained from using a direct non-nulling device.

The direct method has an advantage for application in the various flows encountered, since it will work in laminar, turbulent, or transitional flows and requires no prior knowledge of the flow type.

OBJECT OF STUDY

The goal of this study was to design a simple and reliable skin friction gage that will allow one to directly measure the shear forces on three magnetically levitated train models in Virginia Tech Stability Wind Tunnel.

Recent years have brought a revival of interest in the use of magnetically levitated (MagLev) vehicles (Figure 7) as a means of high speed ground transportation. Maglev vehicles are not a new concept, having being studied in early 1930's in Germany [22]. Maglev systems are currently under investigation in many countries of the world and full scale test and demonstration systems have been constructed in Germany, France and Japan. In the United States, the government support for Maglev has been sporadic. The US MagLev effort was revived in the late 1980's. Sparked by the crowding of the US air transportation system, the National MagLev Initiative (NMI) was formed. NMI, a consortium of federal agencies including the Departments of Transportation and Energy and the Army Corps of Engineers, awarded four System Concept Definition (SCD) contracts for development of a conceptual MagLev design. These four contracts went to Bechtel Corp., Foster-Miller Inc., Grumman Aerospace Corp., and Magneplane International Inc.

In 1993, the Department of Transportation approached NASA for advice on acquiring experimental aerodynamic data. NASA recommended Virginia Tech as the site for wind tunnel testing based upon the quality of the test facilities that are available. Of the four companies initially contracted to pursuit the conceptual design, the Grumman (now Northrop / Grumman) design was the most mature and feasible. During a meeting held at Virginia Tech in April of 1994 with representatives from DOT, NASA, FRA, Northrop / Grumman, and Virginia Tech, it was decided that initial wind tunnel research would use a model of the Grumman design. A moving track system for in ground-effect wind tunnel testing of MagLev vehicles was to be developed for use in the Virginia Tech Stability Wind Tunnel. More specifically, the effect of

vehicle/track aerodynamic interaction on the overall aerodynamic drag was to be investigated. The results from this research would give insight in to the effects of this complex vehicle/track interaction, and they also could be used to aid validation of computational estimates.

In order to take full advantage of the high speed potential of Maglev and to ensure economy of operation, it is important that the aerodynamic drag of the vehicles be minimized. The determination of drag and the other aerodynamic forces is, however, complicated by the fact that the vehicle rides on a track and this track is usually elevated. The aerodynamic analysis of the vehicle alone serves little more than comparative purposes since the vehicle / track interaction will have a significant impact on the aerodynamic behavior of the vehicle.

Several concepts for Maglev system operation exist, each leading to its own type of vehicle design. The two predominate concepts are the electrodynamic suspension system (EDS) which uses a repelling magnetic force to float the vehicle, and the electromagnetic suspension system in which the vehicle undercarriage wraps around the track and an attracting magnetic force is used to suspend the vehicle. Both types of system have been investigated for the use in the United States and abroad. A good overview of the existing and developing Maglev systems is given in [23].

The following chapters will present the process for designing a skin friction balance for flow testing on the Maglev models. Chapter 2 will describe the moving track system for Maglev vehicle / track interaction simulation and the Virginia Tech Stability wind tunnel. In Chapter 3, the design of the skin friction gage utilizing the commercial strain gage unit will be described as well as the processes of gage calibration and C_f calculation. The discussion of the possible sources of error for direct skin friction

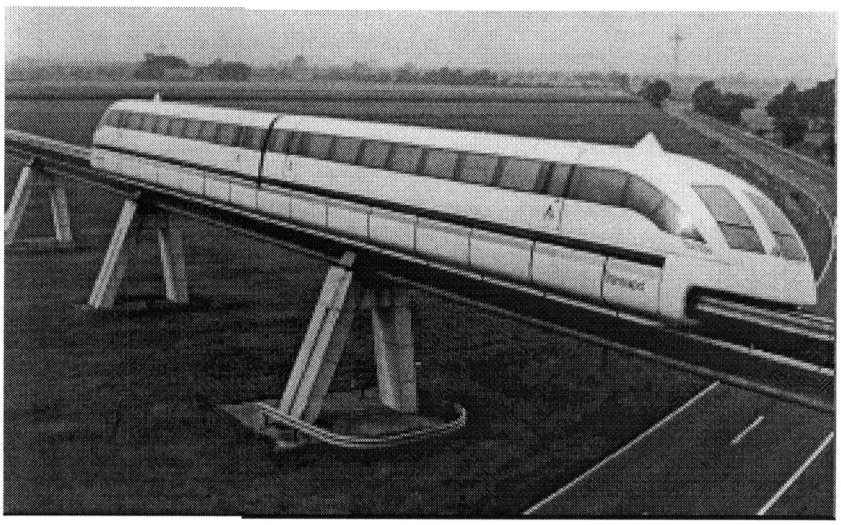

Figure 6. A Current Maglev Design

measurements can also be found in this chapter. Chapter 4 deals with three different Maglev models and the results of the skin friction measurements on these models. Chapter 5 presents an attempt to numerically model the flow in the gap between the vehicle and the track. Conclusions and recommendations for what should be done in future balance designs are given in Chapter 6.

2. EXPERIMENTAL PROCEDURE

MOVING TRACK FACILITY

The aerodynamic behaviour of a ground vehicle is very different from that of an airborne vehicle. Since all aerodynamic forces are due to pressure and skin friction on the vehicle body, any change of these quantities caused by a different flow pattern will lead to a change in the aerodynamic forces experienced. Because of the proximity of the ground, or the vehicle track in this case, to the vehicle, its presence can be expected to have a large effect on the flow pattern. This fact necessitates some method of accounting for the presence of the ground effect during wind tunnel tests.

The most obvious and the simplest method for modeling a ground effect is to place a stationary surface next to the vehicle model in the wind tunnel. However, this method is crude because there exists a relative motion between the vehicle and the ground that is not being simulated. As a vehicle travels down the track, it sees the incoming flow and the track both approach with the same velocity. Thus, no boundary layer is present on the track surfaces. A stationary ground plane in the wind tunnel will develop a boundary layer that does not exist in the real life case. This deviation from the true flow will obviously cause errors in the wind tunnel modeling. This method is generally avoided if vehicle/ground interaction is deemed important.

There are several methods of eliminating the boundary layer associated with the fixed ground plane method. Most

of these methods involve some sort of boundary layer suction or flow injection which causes an imbalance in the conservation of mass for the wind tunnel modeling. In addition, the plumbing necessary to provide for the suction and/or injection also leads to a much more complex apparatus. Unless proper suction/injection is used, which is very difficult to determine and validate, the result is not likely to be satisfactory.

A final method is to have the ground plane in motion, usually using a wide belt. By having the ground plane moving at the same velocity as the air flow, the real life situation is properly simulated. This is the most common method used for automotive wind tunnel testing. This method has some problems modeling the vehicle wheels/tires. Fortunately, with the no-contact criterion for Maglev suspension, this is of no concern in the present test. However, another issue of concern arises here.

All moving ground planes used for automotive testing are intended to simulate the ground. For the case of Maglev, an elevated track needs to be simulated. This comes from the intent of building elevated tracks located above the interstate median, deviating only when necessitated by environmental considerations or road curvatures. This will minimize the costly properties procurement. Because of the need for simulating a moving, elevated track with quality flow both above and below the track surface, the traditional moving ground plane method could not be used. Moving ground plane systems normally used for automotive testing usually require replacing the wind tunnel floor with a wide moving belt. For this investigation, a new apparatus design had to be introduced without causing excessive blockage in the wind tunnel test section.

A moving belt design involving one belt and two pulleys was considered [24]. The whole apparatus was placed inside

the wind tunnel test section instead of having the belt retreating below the tunnel floor. This concept would allow the apparatus to be placed in the wind tunnel without any further modification to the wind tunnel facility. The pulleys must be of sufficient diameter as to separate the distance between the top and bottom sides of the belt, but not so large as to cause excessive blockage of the tunnel section.

Initial research concentrated on the search for commercially available belt systems to simulate the vehicle track. It was determined that in order to minimize Reynolds number differences between the full scale vehicle and wind tunnel model, the moving track must be able to attain a speed as high as possible. An exhaustive search through the market yielded a source that was able to supply a 6 in. wide timing belt that is capable of 134 mph (60 m/s) speed. Figure 7 illustrates the moving track system and vehicle model inside the wind tunnel test section. The choice of using a belt width of 6 in. resulted in a model of sufficient size for force measurement and Reynolds number simulation without causing excessive blockage of the test section. As the belt is widened, the model size must also increase to an extent where blockage will become a problem.

The belt is a self-tracking, timing belt composed of polyurethane with steel tensioners. It is of an endless design in that there is one steel tensioning cable that

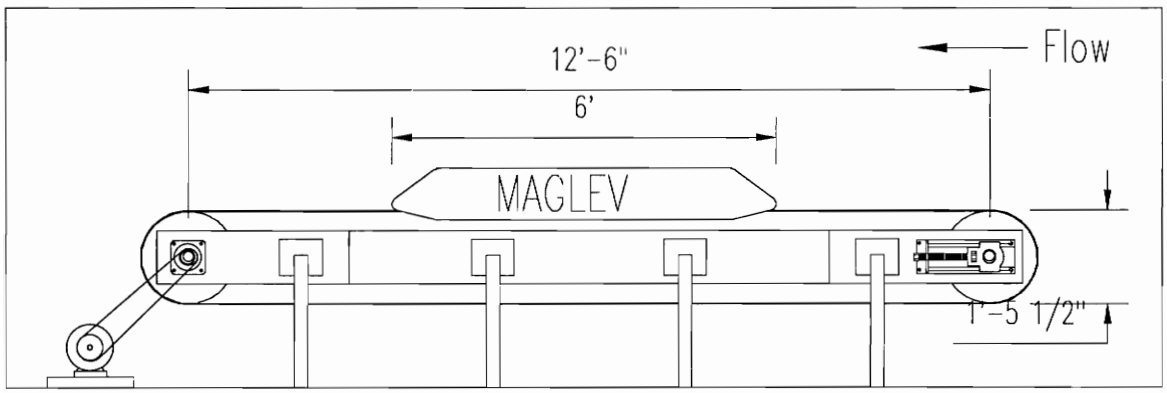

Figure 7. The Moving Track System

winds through the length of the belt. This eliminates any type of joint on the belt and also prevents the typical belt stretching problem. A self-centering tread runs down the middle of belt, mating with a groove in the pulley to provide alignment. The timing belt has a pitch of 0.787 in. (20 mm). This ensures that there will be no belt slippage at high load conditions, thus the speed of the belt is known at all times.

Tests were conducted with the moving track belt system to validate its operation and evaluate its performance. In the initial tests, excessive belt vibration was observed at multiple speeds, including the design speed. The belt manufacturer suggested using slider beds made of ultra high molecular weight polyethylene (UHMW-PE) placed under the belt to prevent vibration. Four slider beds, each 48 in. (1.2m) in length, were placed at adjacent to the belt to minimize belt vibration.

The procedure for matching the speed of the wind and moving belt system began with accelerating the wind tunnel flow to the desired speed after the proper warm-up procedures. Once the wind tunnel was at the proper flow speed as indicated by the Pitot-static probe, the tunnel dynamic pressure, tunnel static pressure, and tunnel temperature were recorded. Using this data, the definition of dynamic pressure, and the ideal gas law, the wind tunnel air speed was calculated as follows:

$$U = \sqrt{\frac{2qRT}{p}}$$

where U is airflow speed q was tunnel dynamic pressure, T was tunnel temperature, p was tunnel static pressure and R was a gas constant for air

Once the tunnel flow speed was known, the corresponding angular velocity of the belt system pulley was then

calculated. This angular velocity was then manually fed into the stroboscope, which flashed at this rate. With the stroboscope aimed at the pulley shaft, the moving belt system was brought up to speed until a marking on the pulley shaft appeared to be stationary. Once this was achieved, the moving belt and the air flow speed were matched.

DESCRIPTION OF STABILITY TUNNEL

The Virginia Tech Stability wind tunnel (Figure 8) is of a single return design. It has a 6 ft x 6 ft x 24 ft removable test section and is powered by a 600 HP electric motor turning a 8 blade propeller of 16 ft diameter. Seven turbulence screens are used to provide a very low turbulence free stream flow. The tunnel has a contraction ratio of 10:1 and a top speed of 250 ft/sec. The Stability Tunnel was originally designed and built at NASA Langley Research Center.

FLOWFIELD VERIFICATION IN THE STABILITY TUNNEL

Since a new experimental apparatus was developed for use in the Virginia Tech Stability Tunnel, its performance needed to be surveyed before further research could be conducted. Questions concerning the effects of the moving belt system on wind tunnel flowfield and blockage had to be addressed prior to studies of the vehicle models.

Flowfield verifications of the moving track system were performed using hot wire anemometry. A single-wire hot wire probe (TSI model 1210-20) was used in conjunction with a

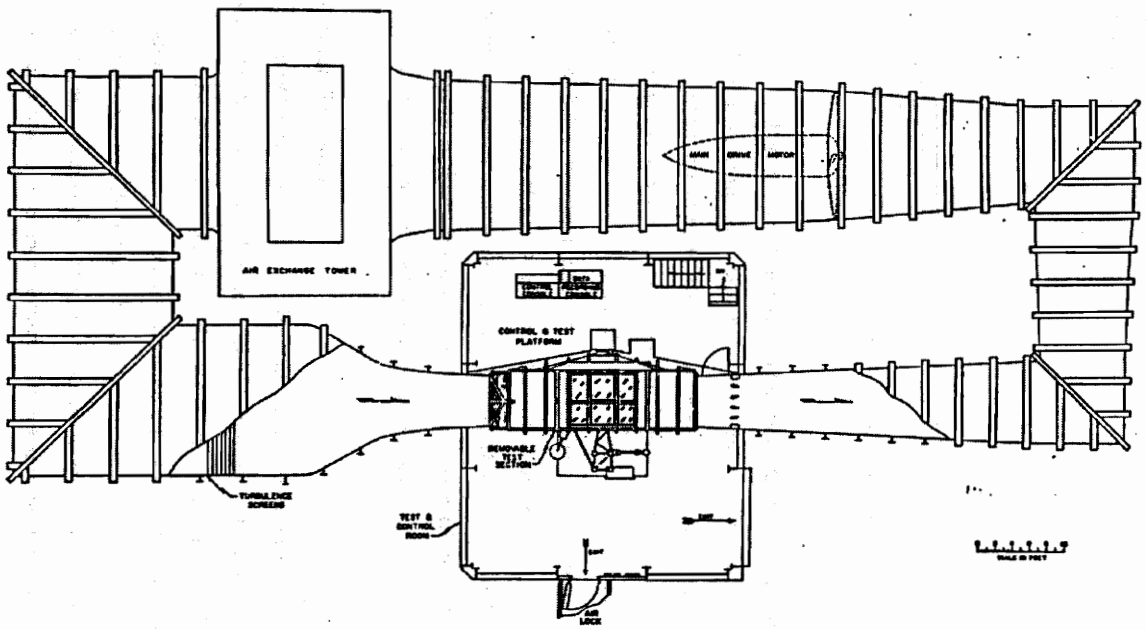

Figure 8. Virginia Tech Stability Wind Tunnel

constant temperature anemometer to measure the flow. Data was collected using a PC computer with a data acquisition board sampling at 1000 samples/second for a length of 2.0 seconds. The hot wire probe was oriented horizontally, to be most sensitive to the flow in the axial direction. It was secured onto a traverse system that allows it to be precisely positioned vertically and horizontally.

The wind tunnel was set to operate at a dynamic pressure of 6 in. of water (120 mph). Measurements were taken both with the moving track stationary and in operation. Velocity profiles at 3 axial locations were taken.

All measurements showed that the flowfield remains quite uniform with the belt system installed in the test section. The boundary layer essentially disappears when the tunnel speed and belt speed are matched. Both of these results indicated that the system will simulate the true flowfield well. See Reference [25] for more details.

Flow conditions are matched between the full and sub-scale vehicles when the Mach number and Reynolds number are the same for both flows. The Mach number, M = U/a, is the non-dimensional ratio of the inertia forces to the elastic forces. The Reynolds number,

$$\mathrm{Re} = \frac{\rho U X}{\mu},$$

is the non-dimensional ratio of the inertia forces to the viscous forces.

For low speed flows, the Mach number is not an important parameter, therefore matching the Mach number for sub-scale tests is not necessary.

Most tunnel designs also make it difficult to match the Reynolds number for these types of tests. A one-tenth model would require testing at ten times the normal speed to match the Re for the same density. This is obviously not

feasible. When the Reynolds number is not matched, the flow at the model's surface is altered, as is the complete flow over the model. Transition of this boundary layer is governed by the value of Reynolds number. Since the model is smaller than on the full-scale vehicle, the Reynolds number will be proportionally lower, therefore the transition from laminar to turbulent flow will occur proportionally farther back on the model than the full-scale vehicle. Trip strips, perturbations in the model surface used to artificially make the flow undergo transition, are added so that the flow over the model correctly simulates the full-scale flow. If the trip strips are effective, the flow will remain similar over a wide range of velocities and so will the non-dimensional values of forces and moment, expressed by coefficients. Trip strips were installed on all models used in this study.

3. GAGE DESIGN

GENERAL DESCRIPTION

The skin friction gage configuration chosen for these experiment was a non-nulling floating element gage. The design is based on the concept that the floating head cantilever arrangement when positioned flush with the surface can produces a deflection that is proportional to the local shear.

Since the flow in this study was subsonic, a very sensitive instrument was required to detect the slight shear forces that are produced by the flow passing tangent to the wall. For example, in a flow with the dynamic pressure q = 750 Pa (which was the case in this study), a typical C_f would give a surface friction force of only about 2 N/m^2. So with a floating head surface area of 10 cm^2, the gage must accurately measure an equivalent weight as small as 0.2 grams.

The general configuration of the designed gage is shown in Figure 9. The floating element responds to shear from the passing tangential flow which is measured by the sensing unit. The sensing head is mounted to the end of the rod, which is a part of the sensing unit. The diameter of the sensing head was chosen 1.5 in (3.81 cm) so that the estimated shear force from the flow will provide enough head deflection for the sensing unit to measure.

One important design issue was that the sensing head must be non-intrusive which means that not only should it

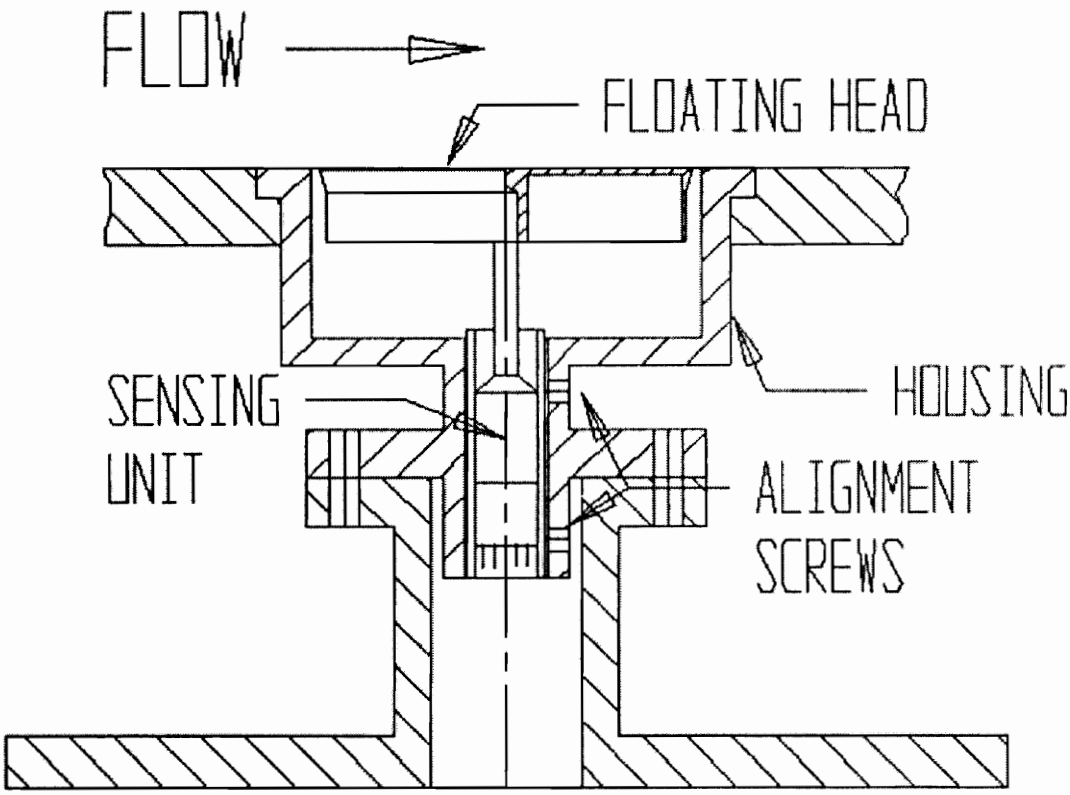

Figure 9. Skin Friction Gage Design.

not protrude above the flow surface, but also it should not recess below the surface, so great attention was paid to the alignment of the sensing head. The sensing unit was placed into a capsule, whose angular position relative to the outer housing could be changed by means of eight alignment screws.

Also, since the potential exists for the local skin friction to be affected by a difference in temperature between the floating element and the rest of the outer wall, the sensing head, gage housing and the gage mounting plate were made of the same material - aluminum.

One of the other issues was the model vibration. Usually, the internal volume of the gage of this type is filled with a viscous fluid to damp the facility vibration and eliminate the effect of the pressure gradients in the flow (Refs [20], [21]). The initial tests of the gage showed that it was difficult to eliminate the spillage of the fluid out of the gap for the sensing head of this size. Since the pressure gradients in the gage location were shown to be negligibly small [23] it was decided not to fill the gage with liquid. Instead, the sensing head was made as light as possible, basically leaving just a skin 0.005 in. thick (see Fig. 9).

Sensing Unit and Test Apparatus

The sensing unit utilized here is a Deflection Sensor Cartridge (DSC®), a complete multipurpose displacement transducer which has the capability of being very sensitive while being stiff. A sketch of the sensing unit is included as Fig. 10. It is a unique piezoresistive strain sensor

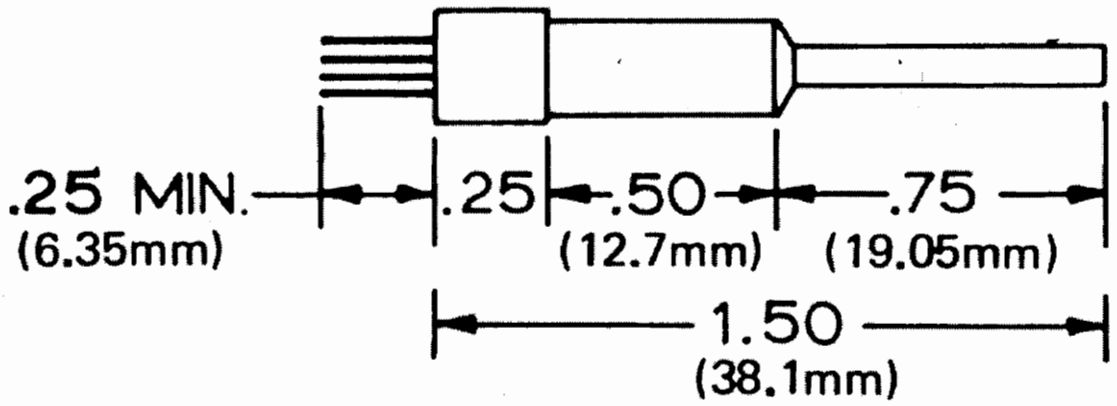

Figure 10. Deflection Sensor Cartridge (DSC®)

used to measure minute deflections caused by a force. As force is applied to the cartridge, two crystals deflect, causing a resistance change. When the crystals are connected in the form of a half-bridge and provided with excitation voltage, a high level output signal, corresponding to the applied force is produced. The DSC consists of a single beam machined from stainless steel with two fiber-like silicon crystals glass-fused into the beam. The DCS is constructed so that the crystal sensors are put into tension and compression simultaneously when the force is applied to the cantilever beam. The two crystals, when wired as the active elements of the Wheatstone bridge, provide a continuous, highly linear signal. The DSC senses the deflection from 0 to ± 0.0381 cm with a linearity of ± 0.05 percent full scale. Note that the forces being measured in this application move the tip of the sensor on the order of 10^{-5} cm, which is at the low end of the range of the sensor.

The standard circuit used for data acquisition as well as for calibration is shown in Fig. 12. The set-up consists of the sensing unit inside the gage connected to the model 2310 Signal Conditioning Amplifier manufactured by Measurements Group, Inc. for the purposes of conditioning and amplifying low-level signals from strain gages or strain gage based transducers. The amplifier incorporates precision high stability resistors for an automatic bridge-completion and balancing. A Keithley-Metrabyte STA-20 Screw Terminal Adapter received the amplified output from the 2310 before sending it to the DAS-20, 12 bit high speed Analog/Digital converter board by Keithley-Metrabyte installed in a i486DX-33 based personal computer. Labtech Notebook® version 8.0 software package by Laboratory Technologies Corp. was used

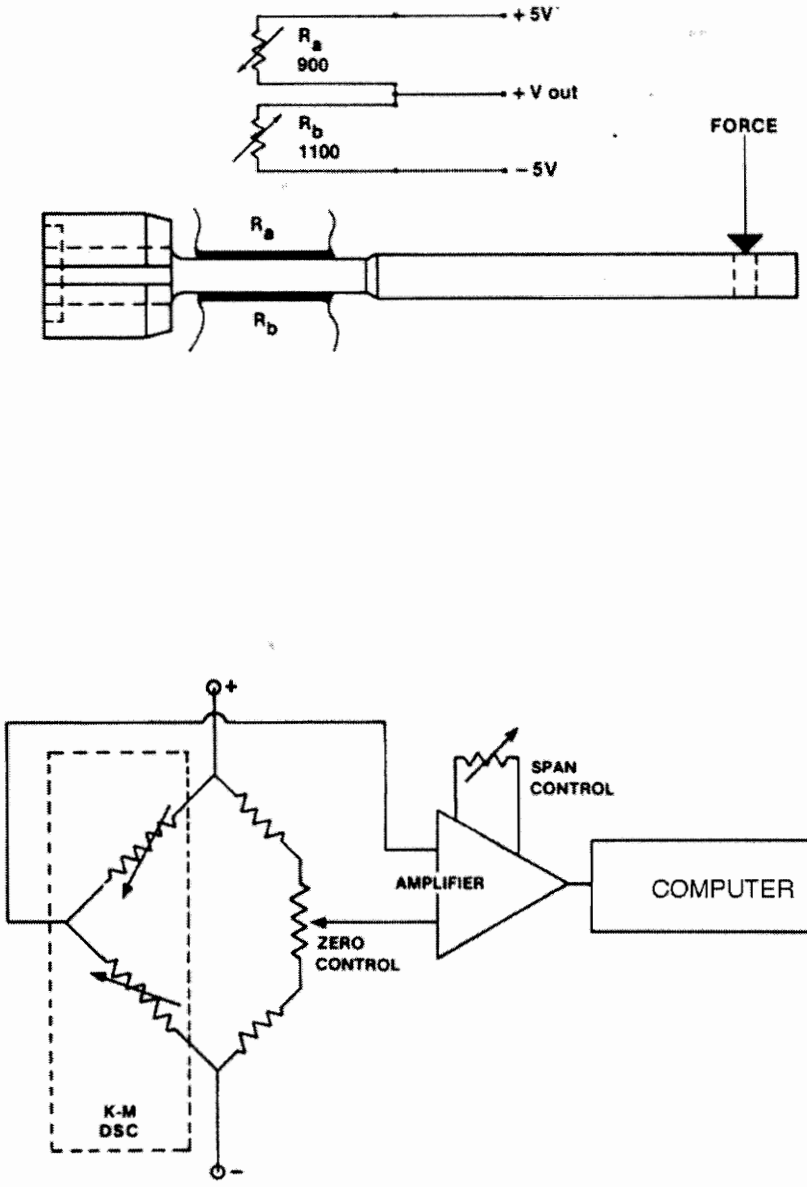

Figure 11. Simplified Wiring Schematic

for data acquisition and processing.

CALIBRATION PROCEDURES

A standard procedure was established for calibration of the gage. A direct force method was chosen, using standard weights and a digital voltmeter. The gage was clamped such that the sensing head surface was in the vertical plane, so that by hanging the weights directly on the sensing head, it was pulled in a streamwise direction. The applied weights ranged from 10 milligrams to 2 grams. The gage will exhibit a linear response in the form:

$$\tau_w = a\Delta V ,$$

where τ_w is the wall shear stress (Force/Head Area), a is a calibration constant and ΔV is the change in the output voltage. A least-squares regression is performed on the calibration data to obtain the calibration curves in volts per gram. These curves are highly linear with the variance on the order of 10^{-4}. Then the calibration is transferred to the units of volts per Pascal of shear force. This is done by multiplying the calibration mass by the gravity acceleration and dividing by the area of the sensing head.

It was very important that the signal return to the same zero after each weight was removed. The drift of the gage was studied carefully and was found not to exceed 0.3 mV in three hours which was approximately 2% of the expected output signal.

A sample calibration curve is shown in Figure 13.

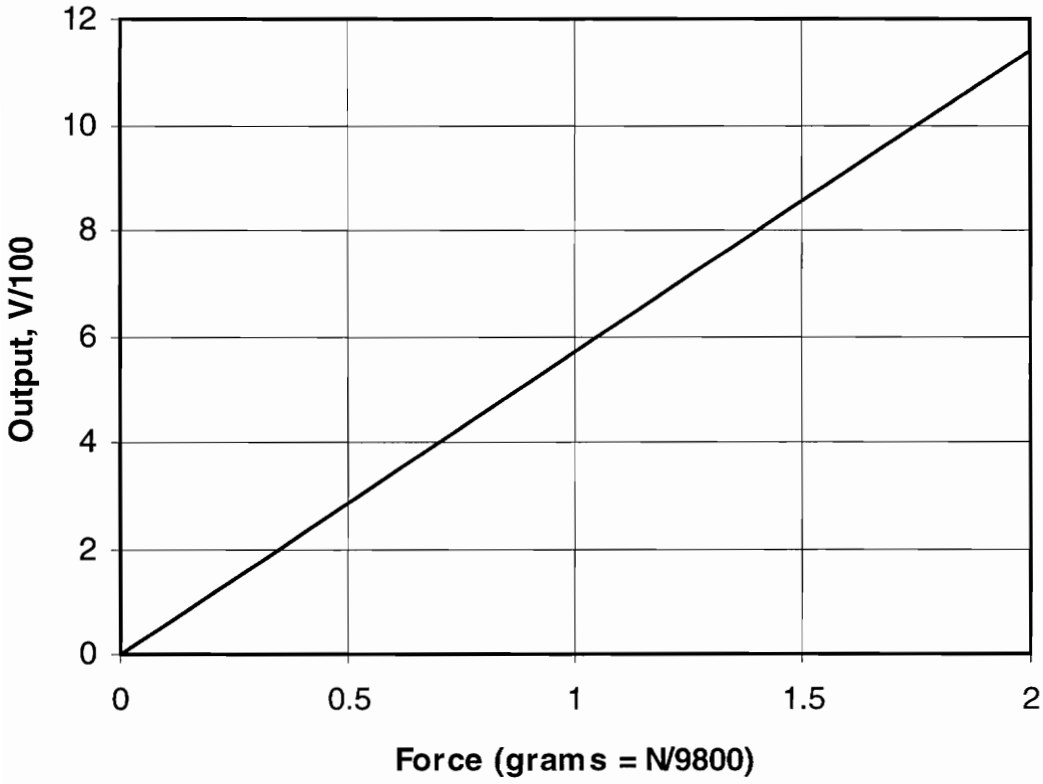

Figure 12. A Sample Calibration Curve

SKIN FRICTION COEFFICIENT CALCULATION.

Calculations of C_f were made using the flow conditions in the tunnel. First, skin friction is defined as

$$C_f = \frac{\tau_w}{q}$$

where τ_w is the shear stress (shear force divided by the sensing head area A = 11.4 cm^2) that is being normalized by the tunnel dynamic pressure $q = 1/2\rho U^2$. It is most desirable use the value of the dynamic pressure that comes from the local boundary layer edge conditions at the location of the skin friction gage, but direct measurements of the dynamic pressure in the flow are not always possible. When these measurements were not available, the freestream value of dynamic pressure was used to normalize the shear force.

GAGE ERROR ANALYSIS

The specific geometry of the floating element is an important design consideration, because it can introduce various potential error sources at the surface. When using a floating element device to measure deflection, misalignment effects are of primary concern. The different possible types of misalignment with the surface and the effect of streamwise pressure gradients are illustrated in Figure 13. Most studies of the effect these parameters are carried out for the supersonic flow. However, we believe that the basic concerns, described in the systematic study carried out by Allen [25] can be applied to this case.

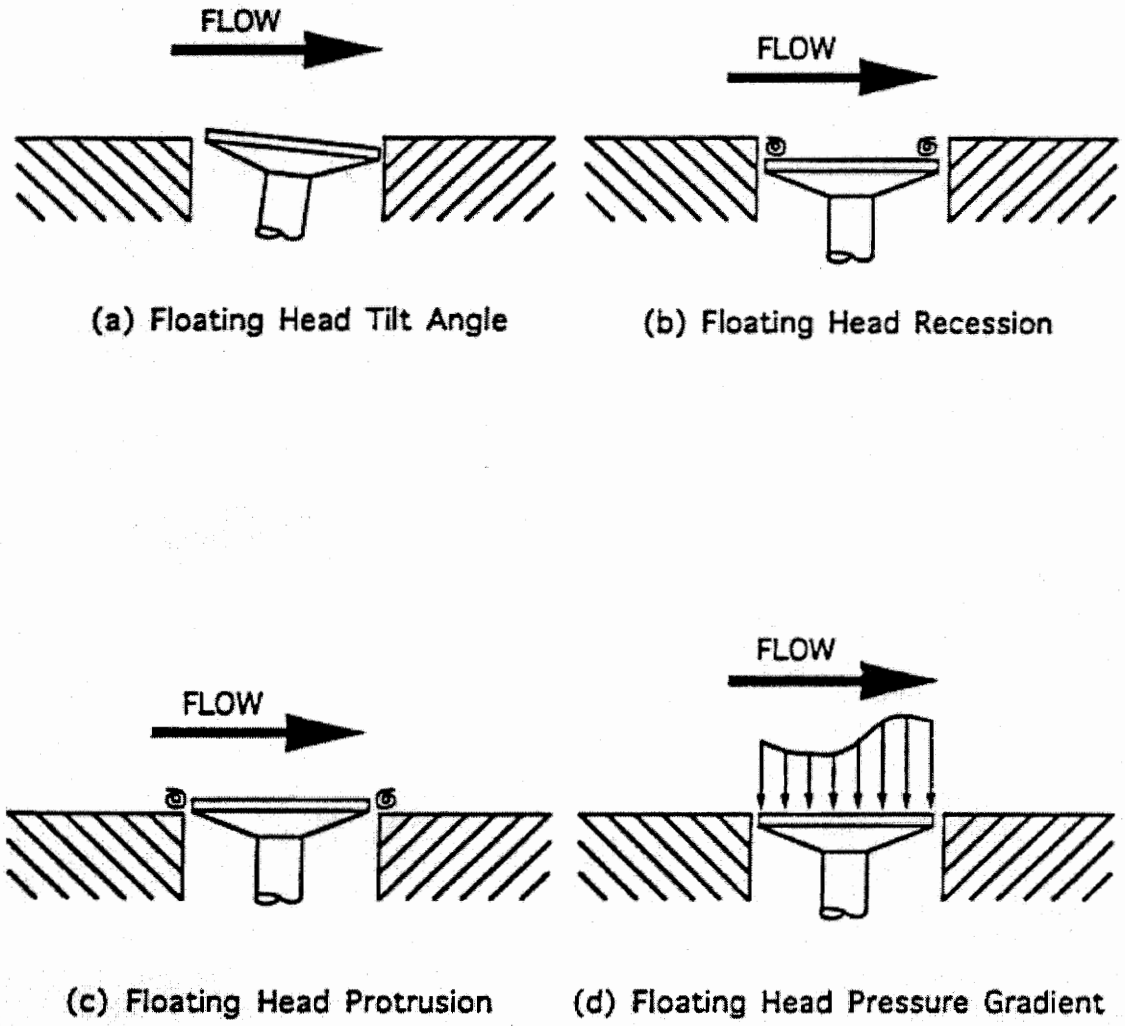

Figure 13 The Possible Misalignment of the Gage

Usually, a non-nulling design carries with it a set of misalignment effects due to the tilt of the floating element into the flow. However, in this case the deflection of the sensing head is so small that the protrusion of the sensing head into the flow is virtually non-existent.

Additional errors can be introduced by the uncertainty of the electronic components in the data acquisition circuit and the errors of the calibration. As mentioned earlier, the zero drift of the gage was studied and found equal to 2% of the full scale signal. The sensitivity to the rotation of the gage was also considered. There is the possibility that during the calibration the sensor axis is not precisely lined up in the streamwise direction. The error of the forward tilt of the gage is found to be 1.5% for small tilt. The error of the gage rotation is a function of the cosine of the angle between vertical and gage sensitivity axes during calibration. The difference in output signal turned out to be less than 2% of the full scale signal for the rotation angle of ±10 degrees. The sensor temperature sensitivity is obtained from manufacturer's specifications applied to the expected output signal. All the possible measurement uncertainties described above are listed below in Table 1.

Table 1. Measurement Uncertainties

Measurement Uncertainties:

1. Transducer uncertainty	
Hysteresis	±2.4%
2. Zero drift	
Uncertainty of electronic components:	
connections, amplifier, computer	±2%
3 Calibration	
Uncertainty due to forward tilt	±1.5%
Uncertainty due to the rotation of gage axis	±2%
Uncertainty due to temperature changes	±3%
4 Sensing Head Misalignment	
Protrusion or Recession	±0.5%
Tilt	±1%
	5.13%

4. SKIN FRICTION MEASUREMENTS

NORTHROP/GRUMMAN MODEL

This MagLev vehicle model geometry was based on designs provided by Northrop/Grumman. The vehicles have a nose that is identical to their tail. This was designed with ease of vehicle operations in mind. Instead of building specialized tracks to turn the MagLev vehicle around for the return trip, the vehicles could simply be operated in the reverse direction. This is a compromise, since a separately designed nose and tail should provide better aerodynamic characteristics. However, since the highest cost of MagLev system is estimated to be the track construction, a reversible vehicle will minimize the capital expense.

The Northrop/Grumman nose shapes were created based on a combination of analytical equations [26]. First, super-ellipses were used to generate the plan view shapes. Side view shapes were then created by connecting piece-wise curves of linear, cubic, and super-elliptic equations. A three dimensional non-wrap-around shape is then completed by fitting super-ellipses at each axial location. The wrap-around section is then generated by 'cutting' out the shape of the guide way, similar to a woodshop routing table operation. By varying parameters within the equations, different shapes were created. The shapes recommended by Northrop/Grumman, and chosen for this investigation were designation number 950 and 1002, as shown in Fig. 14 below. The center body cross-sectional shapes are identical for both vehicles.

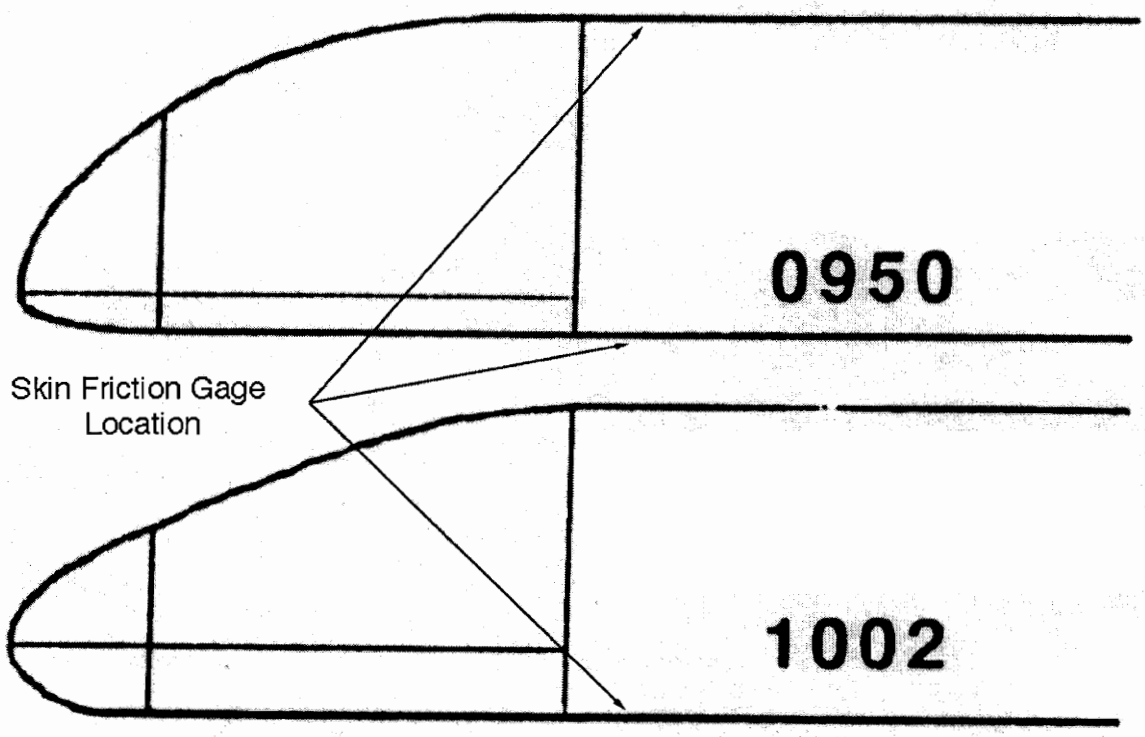

Figure 14. The Shape of the Northrop/Grumman Model

The skin friction gage was installed in two locations on this model. First, it was installed on top of the front part of the center section just aft of the nose section. Later, the boundary layer probe was installed in the same location that allowed us to obtain the boundary layer edge dynamic pressure (see Fig. 15) that was used for calculation of C_f. The first runs showed that the gage produces repeatable output. The sample output of the gage is shown in Figure 16. Table 2 summarizes the results of the first set of measurements and Figure 17 is a plot of C_f versus Reynolds number for the gage installed on top of the model. The Reynolds numbers for this case are based on the width of the model (12 inches)

For the second set of runs, the gage was mounted on the bottom of the center section just aft of the nose facing the moving belt. Since the gap between the model and the moving belt was only 0.47 cm, it was very difficult to locate the boundary layer probe in this gap in order to measure the dynamic pressure. However, the opportunity to estimate the flow parameters in the gap came when the hotwire was used for measuring the velocity and turbulence level in the model wake. Since the wraparound section of the model did not extend all the way to the back, the measurements of the velocity in the middle of the gap could be made This velocity profile shown in Fig. 18 allows us to conclude that the velocity in the middle of the gap on the centerline of the model is very close to the freestream velocity. That is why in all future tests the local shear was non-dimensionalized by the freestream value of the dynamic pressure to obtain C_f.

The tests were run for two proposed nose and tail geometries both In-Ground-Effect and Out-of-Ground Effect. The results of the second set of runs with the gage located at the bottom of the train are presented in Table 3.

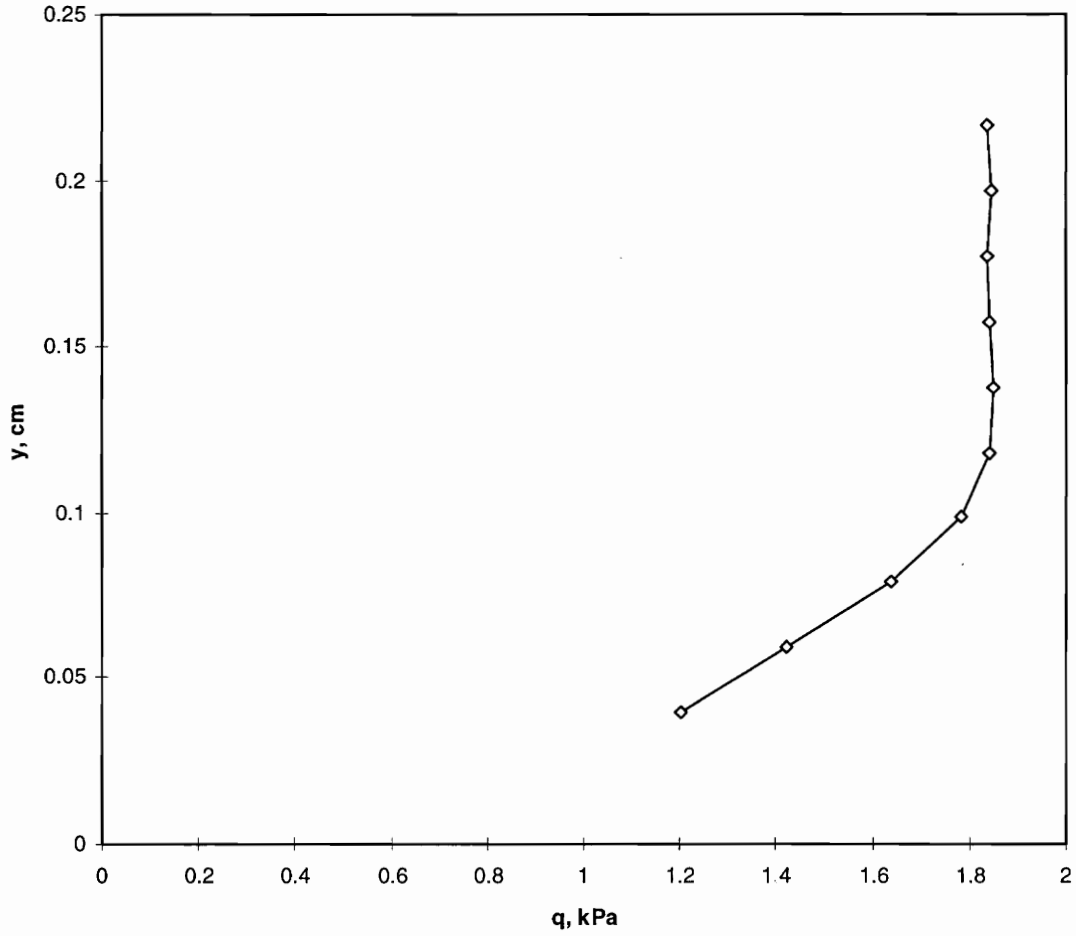

Figure 15. Dynamic Pressure Profile at the Gage Location

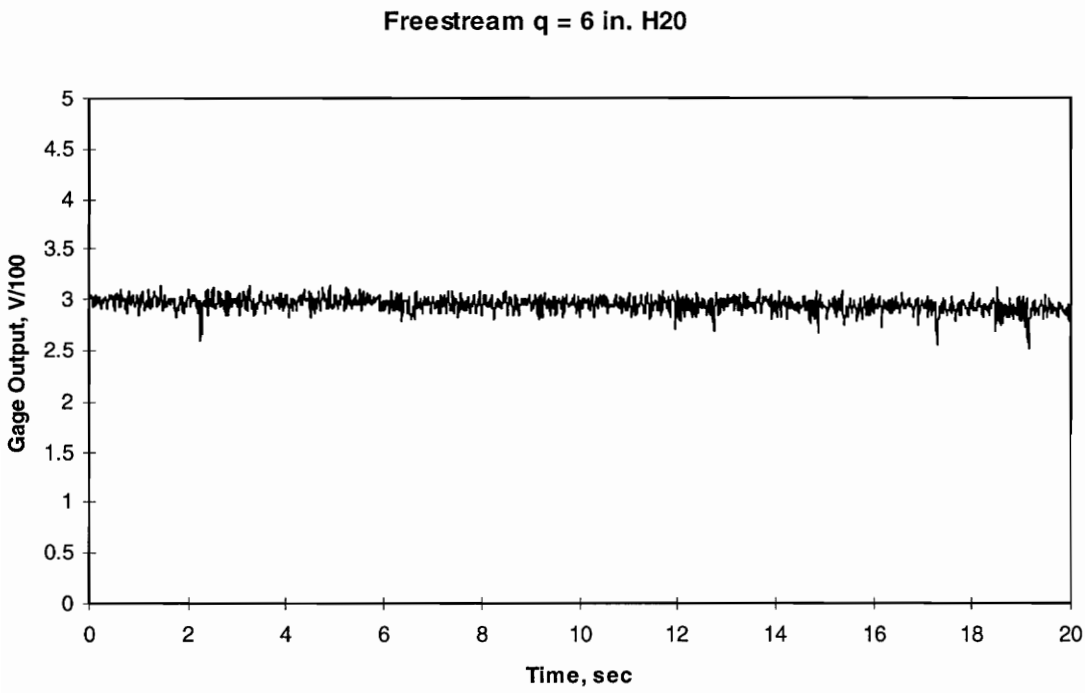

Figure 16. Sample Output of the Skin Friction Gage

Table 2. Skin Friction Measurements on Top Surface of Northrop/Grumman Model

Model	Tunnel q, psi	Tunnel q, kPa	Output, V/100	Shear force,N	Re	C_f
MAG 950	0.2133	1470.65	2.3718	0.00410	7.80E+5	0.00245
	0.2185	1506.51	2.3832	0.00412	7.75E+5	0.00240
	0.2177	1500.99	2.4135	0.00417	7.77E+5	0.00244
	0.1791	1234.85	2.2894	0.00396	7.24E+5	0.00281
	0.1457	1004.57	2.0123	0.00348	6.50E+5	0.00304
	0.0724	499.18	0.9243	0.00160	4.39E+5	0.00281

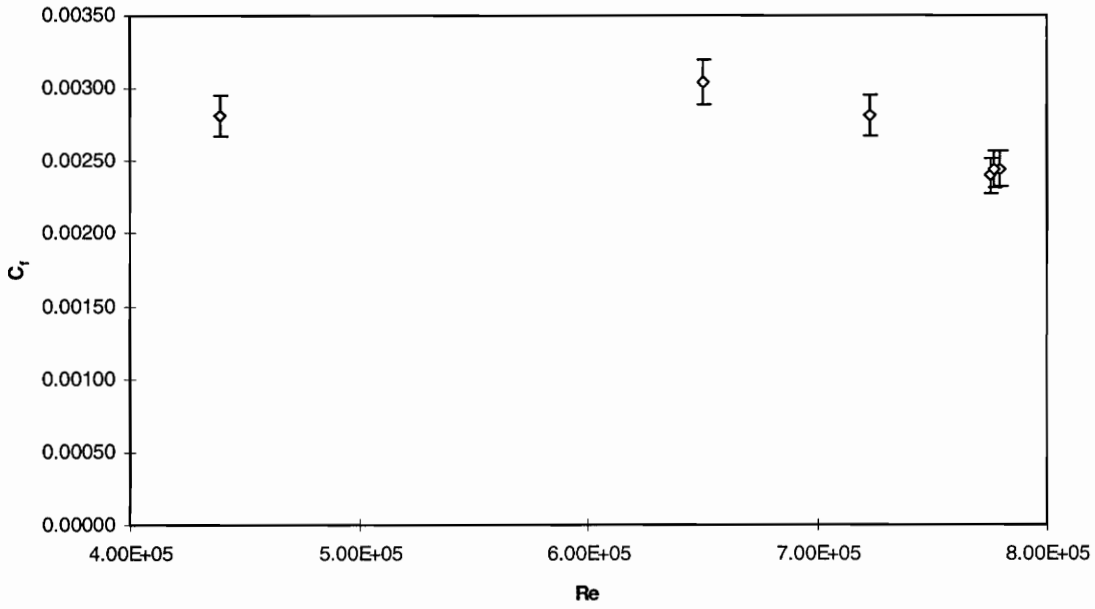

Figure 17. Northrop/Grumman Model. C_f variation with Re.

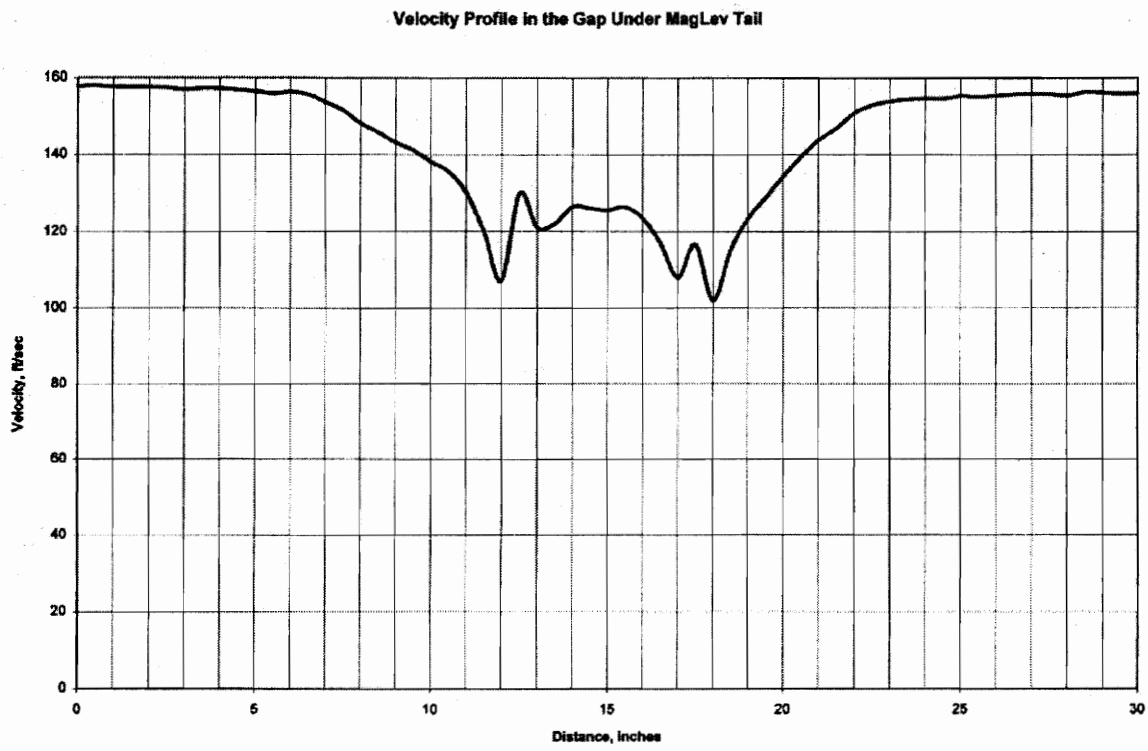

Figure 18. Velocity Profile in the Gap at the Tail

Table 3. Skin Friction Measurements in the Gap.

Model	Tunnel q, psi	Tunnel Q, kPa	Output, V/100	Shear force,N	Re	C_f
MAG950	34.00	1627.87	2.3613	0.00408	1.64E+4	0.00220
	33.90	1623.12	2.0587	0.00356	1.65E+4	0.00192
	34.08	1631.73	2.0207	0.00349	1.67E+4	0.00188
MAG1002	4.60	220.30	0.4294	0.00074	6.00E+3	0.00296
	6.14	293.98	0.6723	0.00116	6.94E+3	0.00347
	8.23	393.88	0.9835	0.00170	8.00E+3	0.00379
	10.33	494.55	1.2533	0.00217	8.96E+3	0.00384
	12.45	596.22	1.5176	0.00262	9.83E+3	0.00386
	14.40	689.61	1.7258	0.00298	1.06E+4	0.00380
	17.57	841.25	2.0622	0.00357	1.17E+4	0.00372
	20.58	985.44	2.5252	0.00437	1.26E+4	0.00389
	23.81	1139.89	2.6384	0.00456	1.36E+4	0.00351
	28.97	1386.87	3.0072	0.00520	1.49E+4	0.00329
	31.21	1494.30	3.2278	0.00558	1.54E+4	0.00328
	34.68	1660.48	3.3376	0.00577	1.64E+4	0.00305

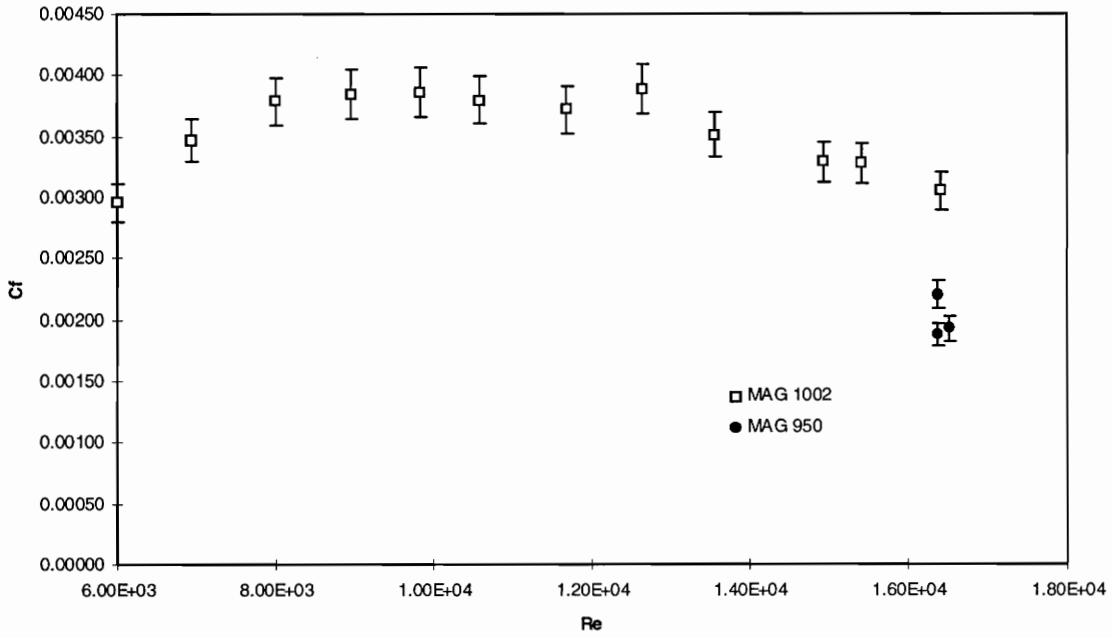

Figure 19. Northrop/Grumman Model. C_f Variation in the Gap.

Here, the Reynolds numbers are based on the distance between the bottom wall of the model and the moving belt (gap height). The variation of C_f as a function of the Reynolds number is shown in Fig. 19.

LOCKHEED/MARTIN MODEL

The model constructed was based on a shape provided by American Maglev of Florida Company. This design was produced by the Lockheed/Martin Corporation. As the belt system pre-existed, the model was scaled so that the track for the full scale vehicle matched the belt width. This criterion led to a 1/16 scale model [27]. Figure 20 shows the geometry of Lockheed/Martin model.

The model is an exact model of the full-scale vehicle, including the slots which run the length of the vehicle for the vertical propulsion rails. For the set-up used for the full model, it was impossible to actually simulate rails running the length of the model. Therefore, the slots were left open during the full model testing. The effect of the vertical rails on the flowfield was studied with a separate model. A line of pins was put in the surface 1.75 inches from the nose. These pins were included to act as a trip strip so that the flow would undergo transition from the laminar boundary layer to the turbulent one. This transition was necessary was necessary so that the measurements on the model would scale correctly to the full-scale vehicle.

Once again the skin friction was installed on the bottom of the center section of the model just aft of the nose facing the belt. As with a Northrop/Grumman model tests were run In Ground Effect and Out of Ground Effect.

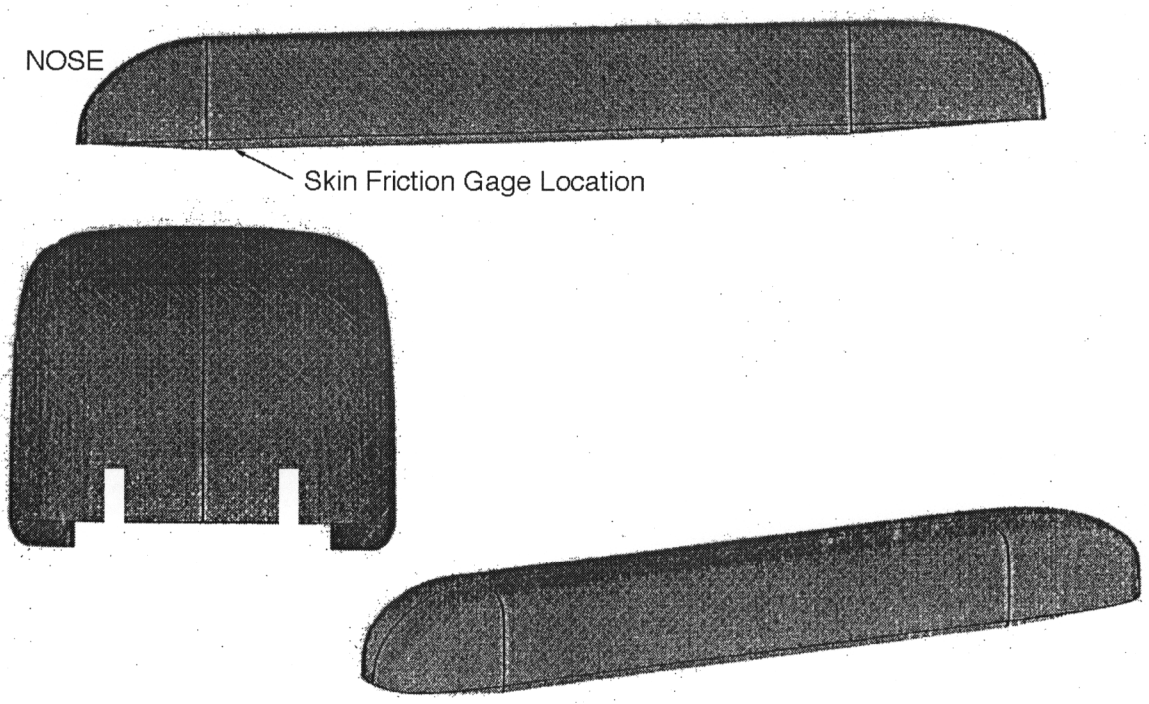

Figure 20. Lockheed/Martin Model Geometry

Table 4. Experimental Results for Lockheed/Martin Model

Tunnel q, psi	**Tunnel q, kPa**	**Output, V**	**Shear Force, N**	**Re**	**C_f**
					IGE
10.50	502.83	0.07	0.0013	1.737E+4	0.0022
14.47	692.84	0.13	0.0023	2.258E+4	0.0029
17.85	854.73	0.12	0.0022	2.451E+4	0.0022
35.00	1675.96	0.28	0.0048	3.166E+4	0.0025
35.02	1676.90	0.28	0.0048	3.151E+4	0.0025
					OGE
10.41	498.39	0.09	0.0016	1.728E+4	0.0028
14.57	697.69	0.12	0.0021	2.035E+4	0.0027
17.73	848.89	0.14	0.0025	2.245E+4	0.0026
20.85	998.20	0.16	0.0028	2.420E+4	0.0025
23.87	1142.72	0.18	0.0032	2.582E+4	0.0024
29.12	1394.37	0.22	0.0037	2.830E+4	0.0023
34.86	1669.02	0.24	0.0042	3.102E+4	0.0022
36.94	1768.90	0.25	0.0044	3.180E+4	0.0022

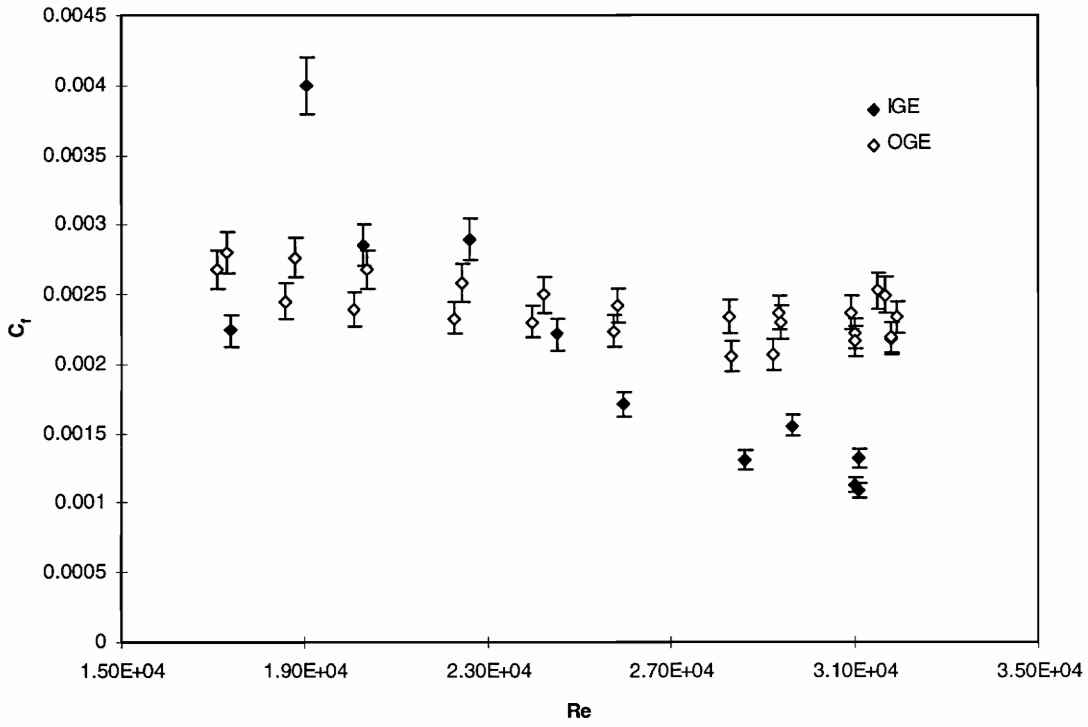

Figure 21. Lockheed/Martin Model. Variation of C_f with Re.

As mentioned earlier the freestream value of dynamic pressure was used to non-dimensionalize the wall shear. The measured values of skin friction coefficient ranged from 0.0022 to 0.0028 over the conditions tested. Table 4 presents a summary of the data collected during the test series with the Reynolds numbers based on the model-belt gap height

Looking at the results, one can see the repeatability of the tests and the skin friction results. The absolute level of the skin friction coefficient measured seems quite reasonable for a turbulent boundary layer at these conditions. Figure 21 shows the variation of skin friction coefficient for the Lockheed/Martin model with the Reynolds number.

PROPULSION RAIL INFLUENCE MODEL

A special model was constructed to study the influence of the propulsion rails on the flow inside the rail slots and around the model. The model was essentially the nose and tail of the Lockheed/Martin train described above without the center section, scaled to match the distance between the rail slots with the width of the existing belt. The model consisted of a bottom with vertical slots which contained all the instrumentation and the top made of the Styrofoam matching the shape of the vehicle. Two large aluminum disks were added on both sides of the rear pulley of the belt system to simulate the moving propulsion rail. Figure 22 shows the "Rail Influence" model installed above the track.

The model was first installed so that the disks entered the slots at the nose. After the skin friction and other

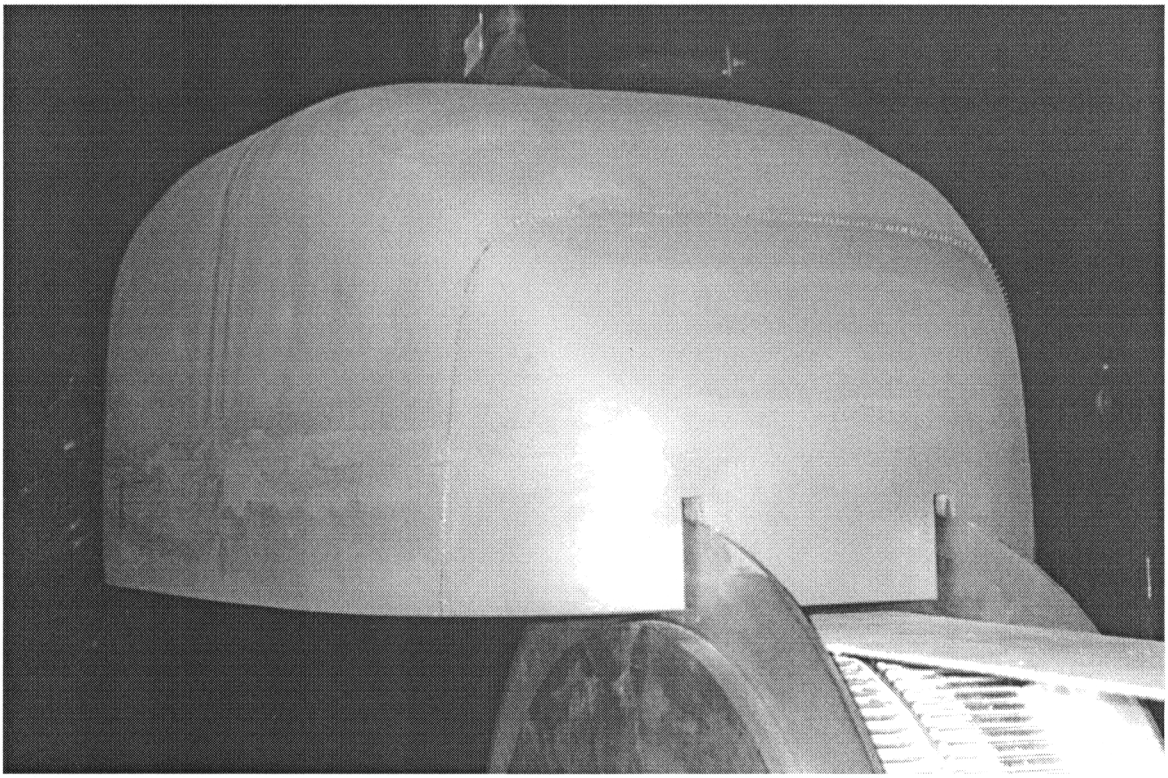

Figure 22. Propulsion Rail Influence Model.

measurements were taken, the model was moved forward so that the disks were located at the exit of the slots.

A skin friction gage similar to one used in the full model tests was installed on the wall of the vertical slot 1.5 inches from the entrance. The scheme of instrumentation setup for measurements inside the propulsion rail slot is shown in Fig. 23. The measured shear force was non-dimensionalized by the tunnel free stream dynamic pressure, which also corresponds to the disk speed.

The data collected during the tests is presented in Table 5. The Reynolds numbers here are based on the distance between the disk and the slot wall (gap width). The measured skin friction coefficient C_f values varied from 0.0026 to 0.0029. The data is reasonable and consistent. These values of C_f were used for comparison with the values obtained in the Couette flow calculations below. The variation of skin friction coefficient with Reynolds number is shown in Fig. 24

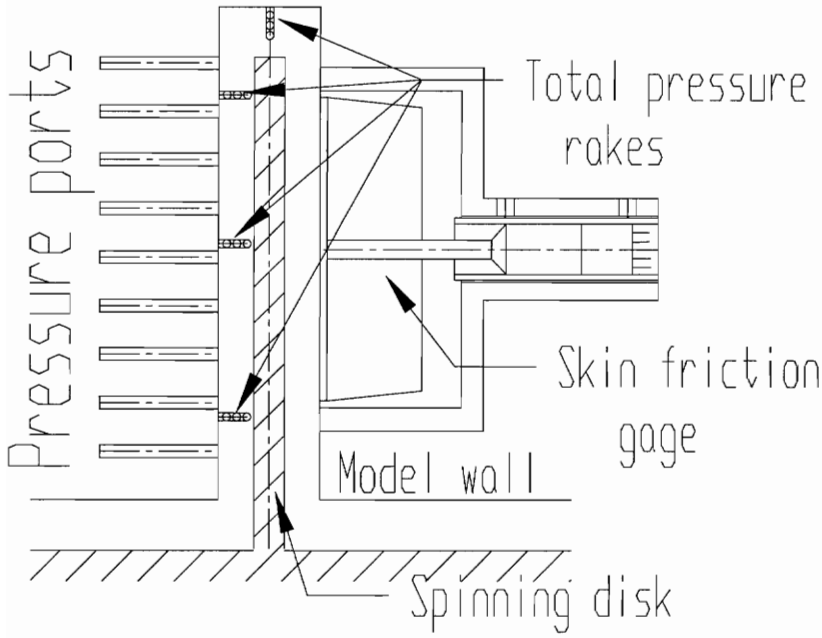

Figure 23. Rail Slot Instrumentation Setup.

Table 5. Skin Friction Measurements in the Slot

Tunnel q, si	Tunnel q, kPa	Output, V	Shear Force, N	Re	C_f
8.76	419.43	0.822	0.00142	4.084E+3	0.00297
20.72	991.89	1.786	0.00309	5.914E+3	0.00273
25.88	1238.94	2.276	0.00393	6.310E+3	0.00279
31.28	1497.63	2.577	0.00445	6.915E+3	0.00261
34.83	1667.72	2.866	0.00496	7.181E+3	0.00261

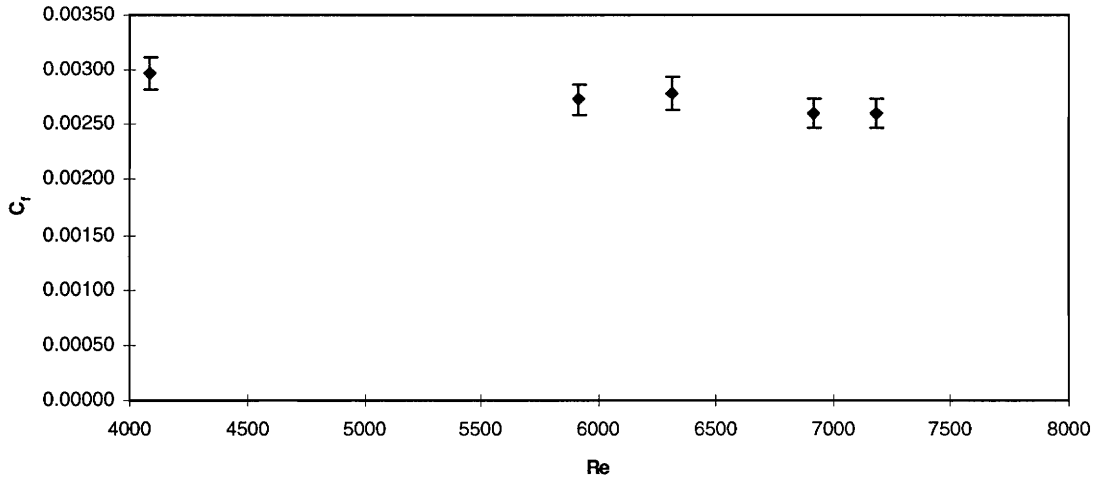

Figure 24. C_f variation with Re in the Slot

5. GAP FLOW CALCULATIONS

The flow in the gap between the vehicle and the track or the vehicle and the vertical propulsion rails is close to the classic Couette flow, except for the fact that there will be some 3-D release from the sides of the gap. Nonetheless, these gap flows were modeled as Couette flows. The following assumptions were made when computing the Couette flow : 1) the flow in the gap is fully developed (which is true for the most part of the flow); 2) there is no cross-flow, i.e. the flow is two-dimensional; 3) there is no axial pressure gradient; and 4) the flow is turbulent and the shear stress is symmetrical about the center of the gap. In all the computations the Reynolds numbers are based on the height of the gap.

A turbulent boundary layer is usually viewed as composite layer consisting of inner and outer regions and the turbulence modeling is different for each of them. The outer models do not predict the slope of the velocity profile away from the walls, while the inner turbulence model alone gives the desired slope of the velocity profile in the core region of the gap [28].

After a careful study of the existing turbulent Couette flow computations, the Reichardt turbulence model was chosen for these calculations. One of the reasons that this turbulence model was selected for these computations was that it does not require evaluating $|\partial U/\partial y|$ as a factor times $\partial U/\partial y$ as in mixing length models.

The equation of motion for the inner region is

$$\tau_w = (\mu + \mu_T)\frac{\partial U}{\partial y}.$$

Integrate this once over the gap height, h, using assumption 4) above to yield

$$U(h) = \int_0^h \frac{\tau_w}{(\mu + \mu_T)} dy \ .$$

Reichardt's form of the eddy viscosity model for the inner region is [3]

$$\mu_T = \kappa \rho \nu \left[\left(\frac{y u_*}{\nu} \right) - y_a^+ \tanh\left(\frac{y u_*}{\nu y_a^+} \right) \right],$$

where y_a^+ is a dimensionless length scale of the order of the laminar sublayer thickness chosen to obtain the best fit with the experiment and $u_* = \sqrt{\tau_w / \rho}$. For the Clauser wall law constants, y_a^+=9.7 with κ=0.41 [4].

Now, these equations can be loaded into a symbolic manipulator such as Matlab™ and the velocity profile can be obtained. Figure 25 represents the velocity profile in the gap between the Maglev train model and the track (h = 0.953 cm and U_{track} = 52 m/s), which corresponds to the tunnel dynamic pressure of 1.8 kPa. The skin friction coefficient calculated for this flow equals C_f = 0.00265 which correlates well with the measurements taken with the skin friction gage (Cf = 0.0025). Fig. 26 shows the velocity distribution inside the slot between the vertical propulsion rail and the slot wall at the same tunnel speed. The slot width is 0.47 cm. The calculation yields the value of Cf = 0.00289, compared to the measured 0.0026. The difference lies within the uncertainty margins for the skin friction gage. The calculations were repeated for the full scale train.

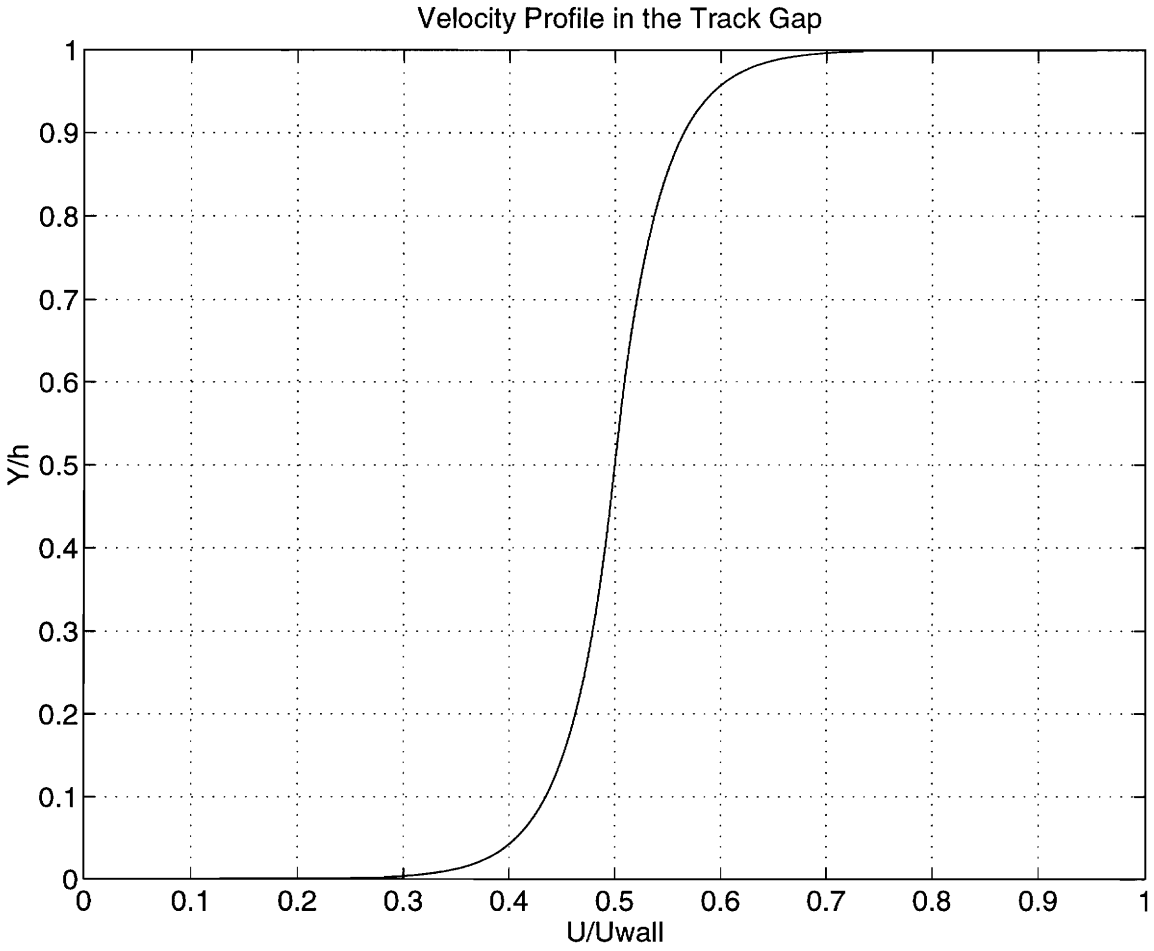

Figure 25. Calculated Velocity Profile in the Track Gap

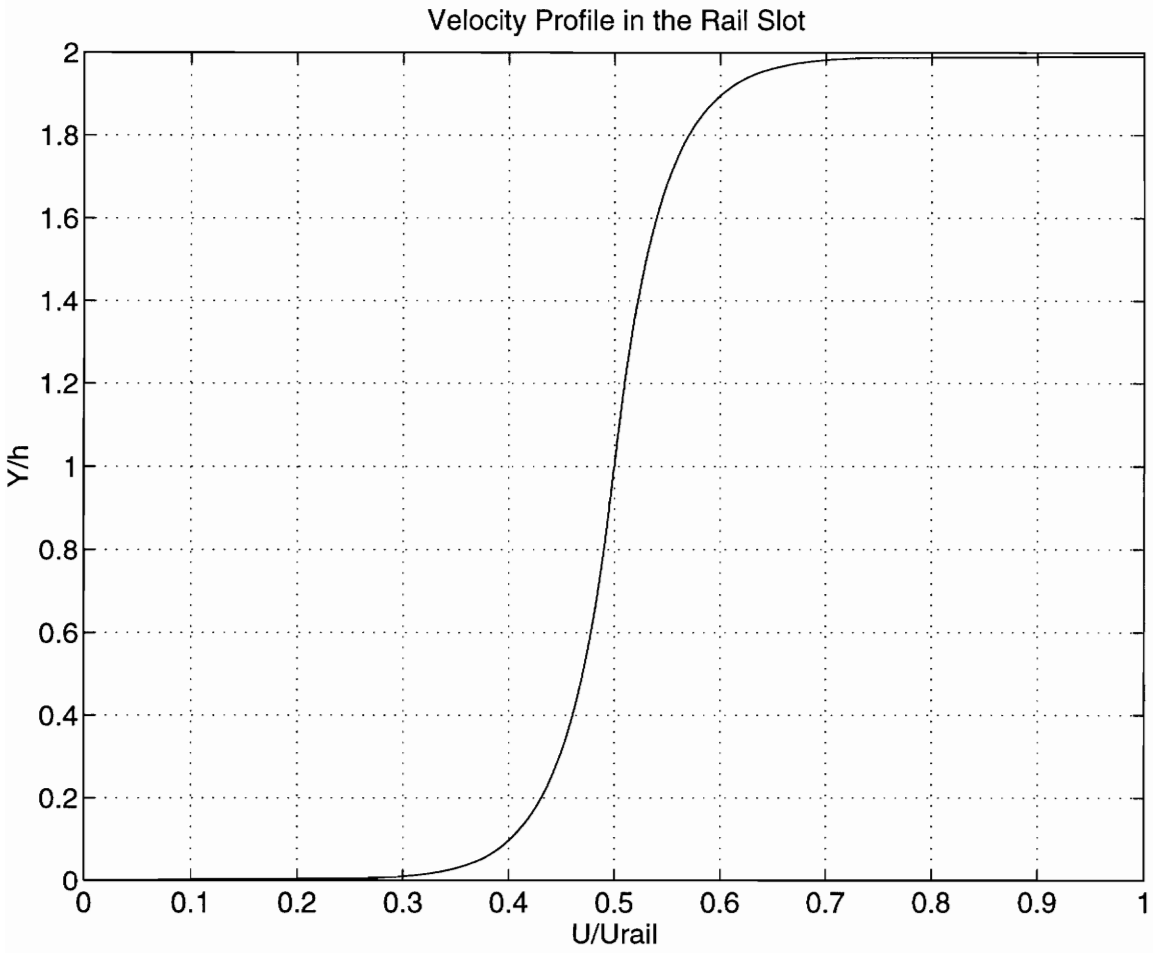

Figure 26. Calculated Velocity Profile in the Rail/Slot Gap

dimensions. The calculated value of the skin friction coefficient for the train speed of 135 m/s was equal 0.00186 for the flow in the track gap (h = 5.08 cm) and 0.00227 for the flow in the rail slot (h = 0.953 cm). These somewhat lower skin friction values can be deemed reasonable cosidering the effect ot the Reynolds number.

6. CONCLUSIONS

The goal to design and build a reliable instrument for the direct measurement of skin friction on the surface of magnetically levitated (MagLev) trains was successfully achieved. The gage utilizes commercially obtained DSC® sensing unit by Kistler Morse. By varying the geometry of the housing of the gage, the design can be adopted for a variety of local wall geometries and test conditions.

Results from several series of tests showed that accurate measurements can be obtained using a cheap and simple, both conceptually and mechanically, skin friction balance. The results of the measurements on different models were consistent and repeatable. Together, this outcome reinforces the validity of the floating element concept for direct measurements of skin friction. An error analysis found the overall uncertainty of the measurement to be within ± 5.3%.

The results of the tests show clearly the influence of the model shape on the skin friction drag for the Northrop / Grumman model suggesting that the 950 model shape will be a better choice. Also, the measurements allow one to see the effect of closeness of the rail track, which result in an overall decrease of the friction in the gap between the model and the track.

Certainly, there is plenty of work to be done. As with any experimental technique, there is always an endless effort to eliminate the errors associated with the measurements. For this gage, lack of accuracy in the calibration leads to most of the uncertainty. Also, the calculated value of skin friction coefficient C_f is only as

accurate as the value of the dynamic pressure q used to non-dimensionalize it. An accurate measurement of local flow properties would add to the accuracy of the calculated C_f values. The use of more sensitive strain gage unit could allow a reduction in the size of the sensing head, that will make the measurements of skin friction more local. In order to use the gage in a flow with high pressure gradients, the inside of the gage's housing should be filled with the viscous fluid which will provide continuity of surface. To eliminate the spillage of the liquid from the gap around the sensing head, the additives that increase surface tension.

Last, to get a total picture of the drag on the magnetically levitated train, there have to be many gages used simultaneously.

BIBLIOGRAPHY

1. Nitsche, W., Haberalnd, C., and Thunker, R., "Comparative Investigations on Friction Drag Measurement Techniques in Experimental Aerodynamics", ICAS-84-2.4.1, 14th ICAS Congress, Sept. 1984.

2. Wooden, P. A., and Hull, G. H., "Correlation of Measured and Theoretical Heat Transfer and Skin Friction at Hypersonic Speeds Including Reynolds Analogy", AIAA Paper 90-5244, Oct. 1990.

3. Schetz, J. A., "Boundary Layer Analysis", Prentice-Hall, 1993.

4. Rubesin, M., "A Modified Reynolds Analogy for the Compressible Turbulent Boundary Layer on a Flat Plate", NASA TN-2917, 1953.

5. Bruno, J. R., "Balance for Measuring Skin Friction in the Presence of Heat Transfer", NOLTR 69-56, June 1969.

6. Gador, A. Y. and Louis, J. F. "High Temperature Heat Transfer and Skin Friction Measurements in Turbulent Flows Along Highly Cooled Walls", AIAA 86-1235, 4th Joint Thermophysics and Heat transfer Conference, June 1986.

7. Owen, F. and Johnson, D. A., "Separated Skin Friction Measurements - Source of Error: An Assessment and Elimination", AIAA 80-1409, 13th Fluid and Plasma Dynamics Conference, July 1980.

8. Bellhouse, B. J. and Schultz, D. L., "Determination of Mean and Dynamic Skin Friction, Separation and Transition in Low-Speed Flow with a Thin-Film Heated Element", *Journal of Fluid Mechanics*, pp. 379-400, 1966.

9. Putz, J., "The Development of Instrumentation for the Support of Skin Friction and Heat Flux Measurements", Ph.D. Thesis, Virginia Polytechnic Institute and State University, 1991.

10. Seto, J. A., and Hornung, H. G., "Internally Mounted Thin Liquid Film Skin Friction Meter Comparison with Floating Element Method Without Pressure Gradient, "AIAA 91-0060, 29th Aerospace Sciences Meeting, January 1991.

12. Seto, J. A., and Hornung, H. G., "Two-directional Skin Friction Measurement Utilizing a Compact Internally Mounted Thin Liquid Film Skin Friction Meter", AIAA 93-0180, 31st Aerospace Sciences Meeting and Exhibit, January 1993.

13. Tanner, L. H., and Blows, L. G., "A Study of the Motion of Oil Films on Surfaces in Air Flow with Application to the Measurement of Skin Friction", *Journal of Physics*, E: Scientific Instruments, pp. 194-202, 1976.

14. Monson, D. J., and Higuchi, H., "Skin Friction Measurements by a New Non-intrusive Double Laser Beam Oil Viscosity Balance Technique", AIAA 80-1373, 13th Fluid and Plasma Dynamics Conference, July 1980.

15. O'Brien, S. A. and Christiansen, W. H., "A Technique for Short-Duration Skin Friction Measurements", AIAA 93-2920, 24th Fluid Dynamics Conference, July 1993.

16. Winter, K. G., "An Outline of the Techniques Available for the Measurement of Skin Friction in the Turbulent Boundary Layers, Progress in Aerospace Sciences, pp. 1 - 57, 1977.

17. Allen, J. M., "Improved Sensing Element for Skin Friction Balance Measurements", AIAA Journal, vol. 18, pp. 1342-1345, November 1980.

18. Vakili, A. D., "A New Skin Friction Balance and Selected Measurements", Experiments in Fluids, pp. 401-406, 1992.

19. Schetz, J. A. and Nerney, B., "Turbulent Boundary Layer with Injection and Surface Roughness", *AIAA Journal*, vol. 15, pp. 1288-1294, September 1973.

20. DeTurris, D. J., A Technique for Direct Measurement of Skin Friction in Supersonic Combustion Flows", Ph.D. Thesis, Virginia Polytechnic Institute and State University, 1992

21. Marshakov, A. V., Schetz, J. A. and Kiss, T., "Direct Measurement of Skin Friction in a Turbine Cascade", Journal of Propulsion and Power, vol. 12, pp. 245-249, 1996.

22. Dickhart, W. W., "The Transrapid Maglev System - an Update" SAE Paper 921583, SAE, Warrendale, PA, August 1992.

23. Liu, D.-J., "Experimental Aerodynamic Comparison of Two Magnetically Levitated (Maglev) Vehicle Designs", MS Thesis, Virginia Polytechnic Institute and State University, 1995.

24. Tyll, J. A., Liu, D.-J., Marchman, J. F., Schetz, J. A., "Experimental Studies of Maglev Aerodynamics", AIAA 95-1917, 13th Applied Aerodynamics Conference, June 1995.

25. Allen, J. M., "Systematic Study of Error Sources in Supersonic Skin Friction Balance Measurements", NASA TN-D-8291, October, 1976.

26. Siclari, M. and Ende, R., "The Application of Navier-Stokes Computations to the Design of High Speed / Low Drag Magnetically Levitated (Maglev) Vehicle Shapes", AIAA 95-1908, 13th Applied Aerodynamics Conference, June 1995.

27. Pulliam, W., Marshakov, A., Tyll, J., Schetz, J. A., Marchman, J.F., "Aerodynamics of the Lockheed/Martin Maglev Train Design", Final Report, VPI-AOE-224, Virgina Polytechnic Institute and State University, 1995.

28. Klopfer, G. H., Mehta, U.B., "Aerodynamic Comparisons for a High-Speed, Magnetic-Flight System", AIAA 95-0749, January 1995.

VITA

Alexei Marshakov was born on April 2, 1996 in Moscow, at that time the capital of the Union of Soviet Socialist Republics. Fascinated by flying machines from his early childhood, he had chosen Moscow Aviation Institute for his undergraduate studies. After graduation, he worked on scramjet research in the Central Institute of Aviation Motors in Moscow for three years. The collapse of the Soviet Union and withdrawal of the "Iron Curtain" have brought him to the United States, first as a visiting scientist and then as a graduate student.